# Electrostatic Deflector Development for Electric Dipole Moment Measurements at Storage Rings

by
**Christian Käseberg**

Master Thesis in Physics

submitted to the
Faculty of Mathematics, Computer Science and Natural Sciences
RWTH Aachen University
in October 2019

written at
III. Physikalisches Institut B

supervised by
**Prof. Dr. Andreas Lehrach**
**Prof. Dr. Lutz Feld**

## Abstract

A major goal of the Jülich Electric Dipole moment Investigations (JEDI) collaboration is to measure the permanent electric dipole moment (EDM) of a proton. This shall be done in a dedicated storage ring which needs electric bending elements. Since no electric bending elements are currently available that can deliver the wanted strength and quality of the electric field they have to be developed and tested.
In this thesis measurements are presented with small electrodes at small distances. These measurement shall show the different behaviour of different materials and coatings at high electric fields. The maximum field strengths that can be achieved with these small electrodes are given and extrapolated to larger distances which are in the region of what will be used in the storage ring.

# Contents


**1 Motivation** **1**

**2 Theory** **3**
2.1 Electric dipole moment . . . 3
2.2 Staged approach of EDM measurement . . . 4
2.2.1 First stage: Precursor experiment at COSY . . . 7
2.2.2 Second stage: Prototype storage ring . . . 7
2.2.3 Third stage: Dedicated EDM storage ring . . . 7
2.3 Electromagnetic fields . . . 8
2.4 Electrical field strength and electrical breakdown . . . 10

**3 The test setup** **13**
3.1 The four electrode pairs . . . 13
3.2 The experimental environment . . . 15
3.3 The measurement procedure . . . 17

**4 Measurement results** **21**
4.1 Behaviour of the dark current for increasing voltages . . . 21
4.2 Reproducibility of the results . . . 26
4.3 Maximum field strengths for different electrodes . . . 29
4.4 Comparison with previous results . . . 38
4.5 Extrapolation for larger distances between the electrodes . . . 41

**5 Conclusion and Outlook** **43**

**Bibliography** **45**

**A Large electromagnetic test bench** **47**

# 1 Motivation

In the last century, a lot of questions in the world of physics could be answered. While these answers led to new problems that have to be solved there are also a lot of other, older problems that need to be studied. One of them is the question why The Universe as we know it contains mainly matter whereas theory predicts an almost equal amount of matter and antimatter.
The Baryon asymmetry can be described by

$$\eta = \frac{n_B - n_{\bar{B}}}{n_\gamma} \text{ [1]} \tag{1}$$

where $n_B$ and $n_{\bar{B}}$ are the number of baryons and antibaryons respectively, while $n_\gamma$ is the amount of photons. The Standard Model (SM) of particle physics does not indicate a significant difference between matter and antimatter. Therefore The Universe is expected to have almost the same amount of matter and antimatter. This corresponds to a predicted value of $\eta \approx 10^{-18}$ [1] for a universe where matter and antimatter are in equilibrium, but the latest measurements give $\eta = (6.14 \pm 0.25) \cdot 10^{-10}$ [2] which clearly indicates an asymmetry.
Andrei Sakharov proposed in 1967, that three conditions need to be fulfilled to create such an asymmetry [3]:

- the Baryon number $B$ must be violated.
- charge conjugation and CP-symmetry both have to be violated.
- there must be reactions out of thermal equilibrium.

While CP-violation is discovered already, the small values that are known as a part of the SM are not large enough to explain the asymmetry between matter and antimatter. A permanent, non vanishing electric dipole moment (EDM) for particles such as protons would mean a further source of CP-violation. Therefore, it could explain the baryon asymmetry in The Universe with beyond the Standard model physics (BSM). Baryon number violation must obviously be fulfilled since no process where the baryon number is conserved can produce more baryons than anti-baryons. The reactions have to be out of thermal equilibrium since an equilibrium would cause the reaction and counter reaction to happen in the same amount. Many experiments are performed to measure permanent EDMs, but up to now no experiment could give a result which is not in agreement with a non vanishing EDM. The current upper limits of different permanent EDMs can be seen in Table 1.

Table 1: Current upper limits for EDM.

| particle | d [e·cm] | date | source |
|---|---|---|---|
| proton | $2.1 \cdot 10^{-25}$ | 2016 | [4] |
| electron | $8.7 \cdot 10^{-29}$ | 2016 | [5] |
| neutron | $3.0 \cdot 10^{-26}$ | 2015 | [6] |
| deuteron | no measurement yet | | |

Up to now the different approaches to measure permanent EDMs were magnetic traps for neutrons [6] or heavier ions [4][7]. The Jülich Electric Dipole moment Investigations (JEDI) collaboration aims to perform these measurements in a particle storage ring with deuterons to get the first limit for the deuteron EDM and later with protons. It is planned to do this in a three staged approach, of which the existing COoler SYnchrotron (COSY) at the Research Center Jülich operated with deuterons is the first stage. The second and third stage shall be done in storage rings that are designed and built especially for the purpose of measuring

the proton EDM. While most modern storage rings have purely magnetic bending sections, a storage ring with either purely electric or combined electric and magnetic bending elements is needed to measure the EDM. A purely magnetic ring is not sufficient since the movement of the spin has to be "frozen" which is only achievable in the presence of an electric field. To achieve the same bending strengths as magnets, the needed electric deflectors have to produce a field in the order of several MV/m. For the size needed, this field is stronger than what is available in industry nowadays. Therefore, investigations have to be made to produce large scale electric deflectors that produce strong enough fields.
While working on the thesis, investigations are made on the influence of different materials and coatings on the field stability with small electrodes. In a first step investigations are made on how the dark current behaves for different types of electrodes. In a second step, the investigations focus on the maximum voltage differences that can be achieved between the electrodes. These measurements are done with the different electrode pairs and for different distances and also compared to previous results. The obtained voltages are used to calculate the maximum achievable fields and the field strength is extrapolated to gap sizes that will be used in a larger test setup (see Outlook) and later the prototype ring.
In general, this thesis is divided into five parts, this motivation being the first of it. The other parts are the following:

- Section 2 deals with the theory of the EDM, the staged approach of the JEDI collaboration to measure the EDM, about electromagnetic fields, electrical field strength and breakdown.
- In section 3 the electrodes and the experimental setup that are used for this thesis are shown. Additionally, the measurement procedure is explained.
- In section 4 the measured data is analysed, compared to previous results and extrapolated for larger gaps.
- Section 5 gives a conclusion of the results. Additionally an outlook on a new experimental setup is given. This setup uses electrodes whose size is closer to the size of electrodes that will be used in the planned storage ring for the second stage of the EDM measurement.

# 2 Theory

This chapter deals with the theory of EDMs and their measurement as well as with electromagnetic fields, the electric field strength and electrical breakdown.

## 2.1 Electric dipole moment

In classical physics, an EDM $\vec{d}$ arises from the separation of positive and negative charge $\pm q$ by a distance $\vec{l}$:

$$\vec{d} = q \cdot \vec{l}. \tag{2}$$

The permanent EDM of subatomic particles is aligned with the spin of those particles since this is the only specified axis in their ground state.
The Hamiltonian operator of such a particle shows that Parity $\mathcal{P}$ and time reversal symmetry $\mathcal{T}$ are both violated:

$$H = -\vec{\mu}\vec{B} - \vec{d}\vec{E}, \tag{3}$$

$$\mathcal{T}(H) = -\vec{\mu}\vec{B} + \vec{d}\vec{E}, \tag{4}$$

$$\mathcal{P}(H) = -\vec{\mu}\vec{B} + \vec{d}\vec{E}. \tag{5}$$

The magnetic field, the magnetic dipole moment (MDM) and the electric field are denoted $\vec{B}$, $\vec{\mu}$ and $\vec{E}$. The breach of Parity and time reversal symmetry can also be seen in Figure 1.

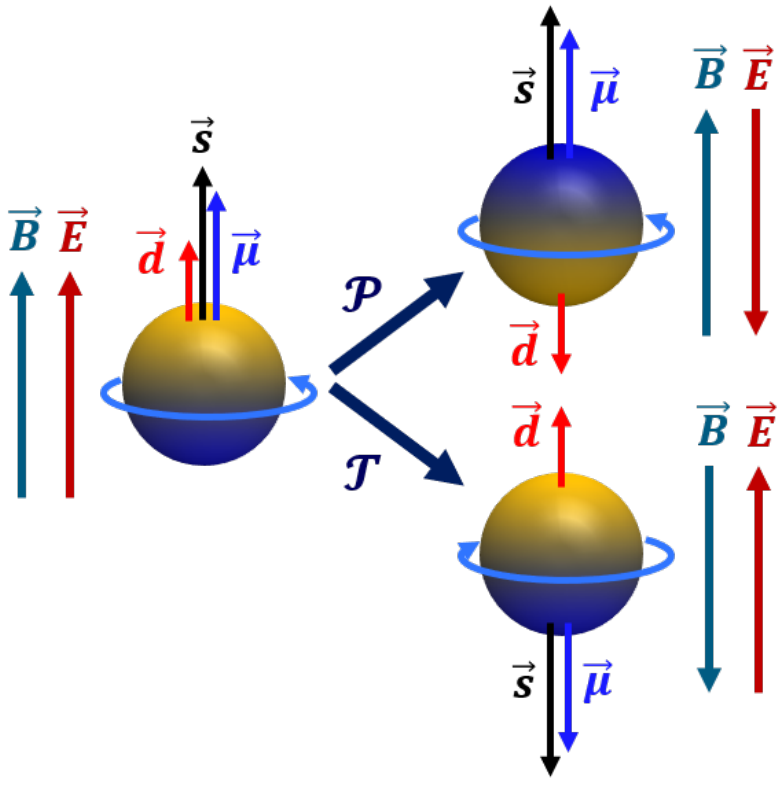


Figure 1: A permanent EDM violates parity and time reversal symmetry [8]. $\vec{E}$ is the electric field, $\vec{B}$ the magnetic field, $\vec{s}$ the spin, $\vec{\mu}$ the magnetic dipole moment and $\vec{d}$ the electric dipole moment. $\mathcal{P}$ describes a parity transformation and $\mathcal{T}$ a time reversal.

Under the assumption that $\mathcal{CPT}$ symmetry holds, any violation of time reversal symmetry directly implies that $\mathcal{CP}$-symmetry is broken. As described in section 1 this is one of the three

Sakharov conditions for baryon asymmetry. Therefore the measurement of a permanent EDM would be a huge step to explain the baryon asymmetry in the universe.
To measure the EDM the time dependent motion of the spin $\vec{s}$ is used. This motion is described by the Thomas-BMT equation. It can be split up to a frequency $\vec{\Omega}_{MDM}$ caused by the MDM and a frequency $\vec{\Omega}_{EDM}$ caused by the EDM[1] [9]:

$$\frac{d\vec{s}}{dt} = \left(\vec{\Omega}_{MDM} + \vec{\Omega}_{EDM}\right) \times \vec{s}. \tag{6}$$

These frequencies are defined as

$$\vec{\Omega}_{MDM} = -\frac{q}{m}\left[G\vec{B} - \frac{\gamma G}{\gamma+1}\vec{\beta}\left(\vec{\beta}\cdot\vec{B}\right) - \left(G - \frac{1}{\gamma^2-1}\right)\frac{\vec{\beta}\times\vec{E}}{c}\right] \tag{7}$$

and

$$\vec{\Omega}_{EDM} = -\frac{\eta q}{2mc}\left[\vec{E} - \frac{\gamma}{\gamma+1}\vec{\beta}\left(\vec{\beta}\cdot\vec{B}\right) + c\vec{\beta}\times\vec{B}\right]. \tag{8}$$

The variables $m$ and $q$ describe the mass and charge of the particle, while $\vec{\beta}$ and $\gamma$ are the relativistic Lorentz factors. The term $t$, $\vec{E}$ and $\vec{B}$ correspond to the time, the electric field and the magnetic field in the laboratory system.
In an ideal particle accelerator, the magnetic and electric fields are all orthogonal to the momentum. With this assumption equations 7 and 8 simplify and they become:

$$\vec{\Omega}_{MDM} = -\frac{q}{m}\left[G\vec{B} - \left(G - \frac{1}{\gamma^2-1}\right)\frac{\vec{\beta}\times\vec{E}}{c}\right], \tag{9}$$

$$\vec{\Omega}_{EDM} = -\frac{\eta q}{2mc}\left[\vec{E} + c\vec{\beta}\times\vec{B}\right]. \tag{10}$$

The MDM $\vec{\mu}$ and the EDM $\vec{d}$ are connected to these equations by the following relations:

$$\vec{\mu} = g\frac{q\hbar}{2m}\vec{s} = (G+1)\frac{q\hbar}{m}\vec{s}, \tag{11}$$

$$\vec{d} = \eta\frac{q\hbar}{2mc}\vec{s}. \tag{12}$$

$G$ and $\eta$ are the so called gyromagnetic anomaly and the dimensionless EDM parameter.
As the magnetic and electric field both have an influence on the spin, it is favourable to choose them in a way such that the net effect on the MDM cancels out and only the EDM influences the spin movement. Depending on the different stages of EDM measurement, this is achieved differently as described in the next section.

## 2.2 Staged approach of EDM measurement

To measure the EDM with storage ring mainly two relevant methods can be used. The first of these methods is the resonant spin method and the second is the frozen spin method. As mentioned before, the JEDI collaboration aims to perform the EDM measurement in three stages, and depending on the stage, a different method is used and achieved differently. The idea of this stages is a result from the Thomas-BMT equation and the desired precision of the measurement. According to equation 6 the motion of the spin is dependent on the MDM, EDM, magnetic field and electric field. To get the highest precision in the EDM measurements it is desirable that all influence of the MDM on the spin cancels out. For this, systematic

[1] In this form of the Thomas-BMT equation, the effect of gravitation influencing the spin movement is neglected. In a real electrostatic storage ring, the gravitation has to be taken into account for design and estimation of the EDM sensitivity.

effects, for example caused by unwanted field components in the ring, have to be taken into account. Therefore the different stages are used to understand this systematic effects better and find ways to reduce them [10].
The first method that can be used is the resonant method. This method can be used in magnetic storage rings. At the injection of the particle beam, the beam is polarized and the spin is parallel to the beam direction. The EDM interacts with the magnetic field and a vertical polarization emerges. At the same time, the vertical magnetic fields in the bending elements interact with the particles' MDM and cause a spin rotation in the horizontal plane. Because of this rotation, the vertical polarization of the spin cancels out again and no net buildup in vertical polarization can be measured. Figure 2 shows the vertical polarization $s_y$ of a polarized particle beam depending on the number of turns in the accelerator.

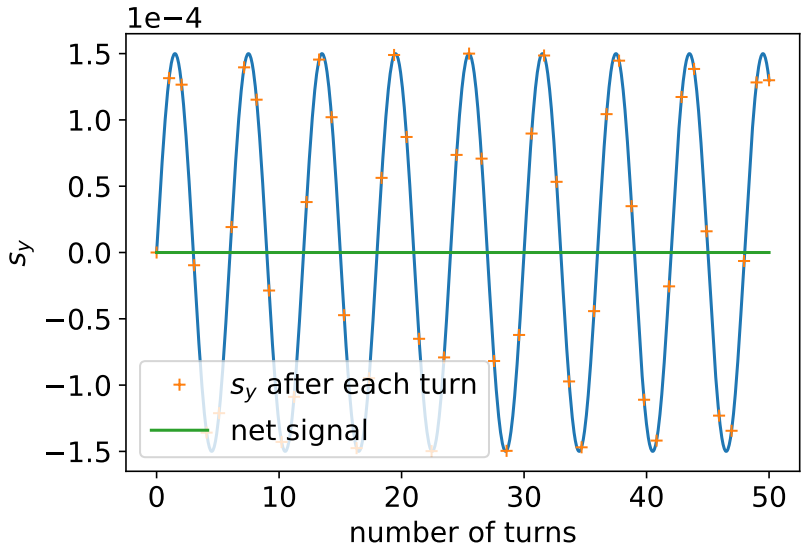


Figure 2: Shown is the vertical polarization $s_y$ caused by the EDM in a magnetic storage ring dependent on the number of turns. The spin tune is chosen to be similar to the COSY spin tune, the amplitude of the oscillation is arbitrary.

It can be seen, that the vertical polarization oscillates around zero. Since the polarization of a particle beam can not be measured for individual turns but only as an average over several turns, no net polarization caused by the EDM, and therefore no EDM, can be measured.
To be able to measure some effect caused by the EDM, a device called radio frequency (RF) Wien-filter (WF) was invented and is installed in COSY [11]. Inside the WF, an electric field and magnetic field are present. The magnetic field is orientated vertically and the electric field is orientated horizontally transverse to the beam direction. Their respective strengths are chosen such that the fields do not influence the beam orbit, but only the spin motion. The fields are chosen time dependent with an oscillation frequency $f_{\mathrm{WF}}$ which is the same as the spin tune frequency or an higher harmonic [11]:

$$f_{\mathrm{WF}} = f_{\mathrm{rev}}|\gamma \mathrm{G} \pm k| \text{ with } k \in \mathbb{Z}. \tag{13}$$

In this equation G is the gyromagnetic anomaly, $\gamma$G is the spin tune and $f_{\mathrm{rev}}$ is the revolution frequency of the particles inside the accelerator.
These fields influence the interaction between the magnetic field in the bending elements and the MDM. The spin gets a kick after each turn and therefore the vertical polarization caused by the EDM does not cancel out. As shown in Figure 3 this leads to a net polarization build up.

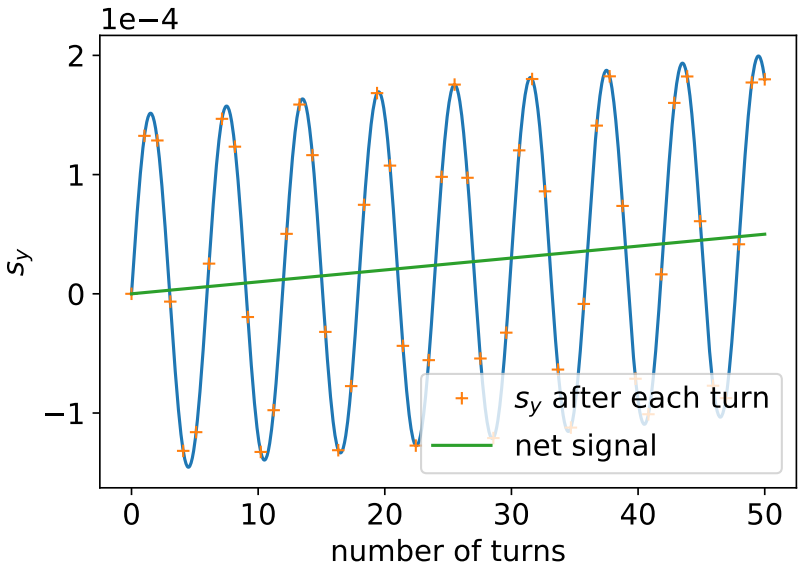


Figure 3: The behaviour of the vertical polarization $s_y$ versus the number of terms in the ring if the WF is included. The fluctuation is not around zero any more but shows an increase over time. The spin tune is chosen to be similar to the COSY spin tune, the amplitude of the oscillation is arbitrary.

This polarization build up over time can be measured and be used to determine the EDM of the particles.
The second way to measure the EDM is the so called "frozen spin" method. This method can be achieved in a storage ring with combined electric and magnetic bending sections or in a fully electric ring. In both cases, the field strengths and particle parameters such as momentum are chosen in a way that influence of the MDM on the spin motion cancels out. Looking at equation 9 for a combined electric and magnetic ring this can be achieved if the following relation holds:

$$G\vec{B} \stackrel{!}{=} \left(G - \frac{1}{\gamma^2 - 1}\right) \frac{\vec{\beta} \times \vec{E}}{c}. \tag{14}$$

For the case that the storage ring has only electrical bending elements, the particle's gamma factor has to be chosen such that

$$G - \frac{1}{\gamma^2 - 1} \stackrel{!}{=} 0 \tag{15}$$

holds. The second way to reach the "frozen" spin also fixes the momentum of the particle. Therefore this approach is called "magic momentum". For protons, this gives a momentum of $p = 700.7\,\mathrm{MeV/c}$ [10], while for deuterons it is not possible because of $G = -0.143$.
In both cases a polarized beam is injected to the storage ring. As the fields are chosen such that the MDM does not influence the spin motion, the whole spin motion is caused by the EDM. If the spin is orientated parallel to the momentum at the injection, the EDM will produce a vertical build up of the polarization which can be measured.
Independent of the method, the polarization of the particle beam has to be measured to determine the EDM. For this, a polarized particle beam inside the particle accelerator is brought to collision with a carbon target. The total cross section $\sigma_{\mathrm{tot}}$ between a polarized beam and a target is given by Equation 16 [12]:

$$\sigma_{\mathrm{tot}} = \sigma_0 + \sigma_{\perp} \vec{P}\vec{Q} + \sigma_{\parallel} \left(\vec{P} \cdot \vec{K}\right) \left(\vec{Q} \cdot \vec{K}\right). \tag{16}$$

In this equation, $\sigma_0$ describes the total spin independent cross section for the hadronic interaction. $\sigma_\perp$ is the spin dependent cross section for the case that the beam orientation $\vec{P}$ and the target polarisation $\vec{Q}$ are transverse, $\sigma_\parallel$ is the spin dependent cross section for the case with longitudinally orientated beam and target polarisation and $\vec{K}$ is the beam direction. Behind the target a polarimeter is placed to measure the distribution of the scattered particles and therefore their polarization. While the procedure to measure the polarization is done the same for the three planned stages of EDM measurement, the particles, the accelerator and especially the type of used bending elements in the accelerator vary for the different stages [10].

### 2.2.1 First stage: Precursor experiment at COSY

The first stage of measuring the EDM is the precursor experiment. As COSY is a synchrotron with purely magnetic bending sections, the only possible way to measure the EDM is with the resonant method. COSY has a spin tune of $\nu_{\text{spin}} \approx 0.161 \approx 1/6$ and a revolution frequency of 750.2 kHz for deuterons with a momentum of 970 MeV/c [11]. To measure the deuteron EDM, the RF WF was designed and installed in COSY. Compared to the COSY circumference of 184 m the length of the WF is only 0.9 m and therefore smaller by a factor 200 [11]. This limits the polarization buildup caused by the WF and therefore the statistical precision of the EDM measurement. Still, this will be the first ever measurement of the deuteron EDM.

### 2.2.2 Second stage: Prototype storage ring

To reduce systematic effects caused by the MDM and the magnetic fields, as well as to increase the effect of the EDM on the spin motion, a dedicated ring for EDM measurements is needed. Therefore the second stage of EDM measurement is the so called prototype ring [10]. This ring is mainly planned to test experimental methods for a later accelerator. The prototype ring will use combined bending elements that can produce an electric field and a magnetic field to deflect the accelerated polarized protons inside the ring. The prototype shall be used in two modes. In the first mode, only electric bending will be used. This allows to have two counter rotating beams at the same time in the ring. The use of two counter rotating beams is needed for future EDM measurements to decrease systematic uncertainties caused by asymmetric effects. In particle colliders this was achieved with magnetic bending elements up to now. Since the use of electric bending elements is necessary for the EDM measurement, but also new for a storage ring, it has to be studied how to control these two beams simultaneously. In this mode the protons have an energy of 30 MeV and no EDM measurements will be done. The second mode of the prototype ring uses electric and magnetic bending sections which allows only one beam in the accelerator at a time[2]. The desired proton energy in this stage is 45 MeV as equation 14 cancels out and the spin 'freezes'. Therefore this stage will give a measurement result of the proton EDM.

### 2.2.3 Third stage: Dedicated EDM storage ring

Once the prototype ring gives enough feedback of handling two beams, systematic errors etc., the target is to finish the planning of the final ring and build it. This ring will accelerate protons and feature electric bending elements only but no magnets. With this ring it is planned to perform proton EDM measurements up to a limit of $d = 10^{-29}\,\text{e} \cdot \text{cm}$. Two counter rotating beams of protons are circulating simultaneously in the ring. These two beams will reduce systematic effects in the ring like fringe field effects or effects caused by not perfectly aligned fields. The two beams in this ring will have the so called 'magic-momentum'. This

[2] Still, it will be possible to flip the magnetic field and do another run with a beam circulating in the opposite direction to minimize the error.

means that the momentum, and therefore the $\gamma$-factor are chosen in a way that equation 15 holds. For protons who have a gyromagnetic anomaly of $G = 1.793$ this corresponds to a momentum of 700.7 MeV/c. For deuterons it is not possible to operate at magic momentum, since the gyromagnetic anomaly is $G = -0.143$ and therefore equation 15 can not hold.

Key facts of the different rings and therefore of the three different stages are shown in Table 2.

Table 2: Parameters of the three different rings. For the prototype ring, the type of bending, the number of beams or the energy are dependent which of the two operation modes is chosen. Values marked with $\sim$ or a * are dependent on the final design or up to the design.

| | COSY [13] | prototype ring [10] [14] | final ring |
|---|---|---|---|
| strategy | precursor | test/measure | measure |
| mode | resonant | frozen spin | frozen spin |
| particle | deuteron | proton | proton |
| circumference [m] | 184 | $\sim$ 100 | $\sim$600 |
| bending elements | magnetic | el. mag./electric | electric |
| bending radius [m] | 7 | $\sim$ 8.86 | * |
| bending field | max 1.7 T | 5-10 MV/m + 40 mT | * |
| # of beams | 1 | 2 or 1 | 2 |
| E [MeV] | 2111 | 30 or 45 | 1175 |
| p [MeV/c] | 970 | 239 or 294 | 700.7 (magic) |

## 2.3 Electromagnetic fields

Between 1861 and 1864 James Clerk Maxwell formulated four equations to explain the behaviour of electric and magnetic fields. These equations describe the behaviour of these fields for the static case but also for the time dependent case, where electric fields induce magnetic fields and vice versa. The equations are named Maxwell equations and are the following [15]:

$$\nabla \cdot \vec{E} = \frac{\rho}{\epsilon_0}, \tag{17}$$

$$\nabla \cdot \vec{B} = 0, \tag{18}$$

$$\nabla \times \vec{E} = -\frac{d\vec{B}}{dt}, \tag{19}$$

$$\nabla \times \vec{B} = \mu_0 \left( \vec{J} + \epsilon_0 \frac{d\vec{E}}{dt} \right). \tag{20}$$

In these equations, $\nabla$ is the nabla operator, $\rho$ the electric charge density, $\epsilon_0$ the permittivity of vacuum, $\mu_0$ the vacuum permeability and $\vec{J}$ the electric current density. They are connected with the speed of light $c$ via

$$c = \frac{1}{\sqrt{\mu_0 \epsilon_0}}. \tag{21}$$

As they are fundamental equations of electromagnetic fields, a lot of conclusions can be taken from them [16]:

- The first of the equations, equation 17, is the Gaussian law. It says that the divergence of the electric field is the same as the electric charge density divided by $\epsilon_0$. In an alternative writing it says that the net current through a closed surface that encloses a electrical charge, is in total equal to the charge inside the surface.

- Equation 18 is the not existence of magnetic monopoles. Opposing to electric fields, where single monopoles exist, there are no monopoles but only poles of higher order for magnets.
- Equation 19 is Faraday's Law of induction. It states that any time changing magnetic field also induces a non conservative electric field.
- Equation 20 is Maxwell's version of Ampere's law. It says that any electric current or any change of an electric field also induces a magnetic field.

The last two equations connect electric and magnetic fields. This shows that they both are able to influence each other and that time dependent problems can become very complex. The other important part to describe electromagnetic effects is the Lorentz force $\vec{F_L}$. The combination of Maxwell equations and Lorentz force is able to explain all parts of fundamental electrodynamics. The Lorentz force describes the force that an electric field $\vec{E}$ and a magnetic field $\vec{B}$ perform on charged particles, such as protons or deuterons in a particle accelerator. It is given by [15]

$$\vec{F_L} = q\left(\vec{E} + \vec{v} \times \vec{B}\right). \tag{22}$$

The charge of the particle is denoted $q$ and $v$ is the particles velocity. The change of the kinetic energy $T$ of a particle caused by an external force is given as

$$\begin{aligned} \frac{dT}{dt} &= \frac{d}{dt}\frac{1}{2}m\vec{v}^2 && (23)\\ &= m\vec{v}\cdot\dot{\vec{v}} && (24)\\ &= \vec{v}\cdot(m\vec{a}) && (25)\\ &= \vec{v}\cdot\vec{F}. && (26) \end{aligned}$$

With the particle's mass denoted as $m$, the velocity as $\vec{v}$, the acceleration as $\vec{a}$ and the force as $\vec{F}$. Inserting equation 26 into equation 22 gives

$$\begin{aligned} \frac{dT}{dt} &= \vec{v}\cdot\left[q\left(\vec{E} + \vec{v}\times\vec{B}\right)\right] && (27)\\ &= q\vec{v}\cdot\vec{E} + q\vec{v}\cdot\left(\vec{v}\times\vec{B}\right) && (28)\\ &= q\vec{v}\vec{E}. && (29) \end{aligned}$$

The last expression in equation 28 is equal to zero since $(\vec{v}\times\vec{B}) \perp \vec{v}$ holds and therefore the scalar product is zero. As a consequence, the particles' kinetic energy and therefore the absolute value of the velocity can only be changed by using an electric field and not by use of a magnetic field.
The Lorentz force can therefore be split up into an electrical part $\vec{F_{L,e}}$ and a magnetic part $\vec{F_{L,m}}$:

$$\begin{aligned} \vec{F_{L,e}} &= q\vec{E}, && (30)\\ \vec{F_{L,m}} &= q\vec{v}\times\vec{B}. && (31) \end{aligned}$$

As shown above to accelerate a particle only the electric field can be used. To deflect a particle, electric field and magnetic field can both be used. To do so the electric field has to point in the direction where the particles shall be deflected. The magnetic field must be

orientated perpendicular to the velocity of the particle and the desired direction. Therefore it has to be orientated vertically in particle accelerators.
Due to technical reasons mainly magnets are used in today's particle accelerators, since the needed fields are much easier to produce with magnets than with electrodes. COSY in Jülich is operated with deuterons at a momentum of 970 MeV/c for the precursor experiment, which corresponds to $\beta = 0.459$. The magnets used can produce a field of up to 1.67 T and have a bending radius of 7 m. The same bending radius could be achieved using an electric field of $64\,\frac{\mathrm{MV}}{\mathrm{m}}$. While the strength of the magnets can be reached easily, an electric bending element with such high fields is not easy to achieve. For the measurement of the proton EDM in the prototype ring, the particles' momentum is planned to be below 300 MeV/c. Therefore the electric fields do not have to be as high as in this hypothetical case for COSY and it is possible to use electric bend elements. Magnets can not be used for bending in the prototype ring since their field influence the EDM measurement. This is a result of interaction between the magnetic field and the magnetic dipole moment, as explained in detail in section 2.1.

## 2.4 Electrical field strength and electrical breakdown

The electric field strength $E$ between two electrodes is described by [17]

$$E = f \cdot \frac{U}{d}. \tag{32}$$

The distance between the electrodes is denoted $d$ and the applied voltage is $U$. The dimensionless field enhancement factor (FEF) $f$ is introduced to take the shape and geometrical effects of the electrode into account. For two electrodes formed as half spheres with a radius $r$ the factor is given by [17]

$$f = \frac{1}{4}\left(1 + \frac{d}{r} + \sqrt{\left[1 + \frac{d}{r}\right]^2 + 8}\right). \tag{33}$$

The electrodes that are used for the measurements for this thesis are half spherical, have a radius of 10 mm and the distance between the electrodes varies between zero and one millimetre. The values of $f$ for gaps of this size are shown in Figure 4.

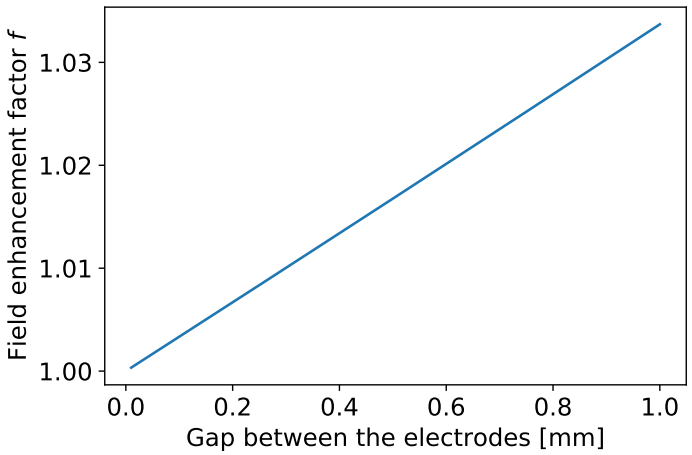


Figure 4: The behaviour of the field enhancement factor for the used set of electrodes and distances.

This figure shows, that the relative variation of the factor is below 3%. Additionally it can be seen, that the behaviour is almost linear. To show the deviation from the linear

behaviour, the difference between the actual line and a linear connection between $f(0.01\,\mathrm{mm})$ and $f(1\,\mathrm{mm})$ is shown in Figure 5.

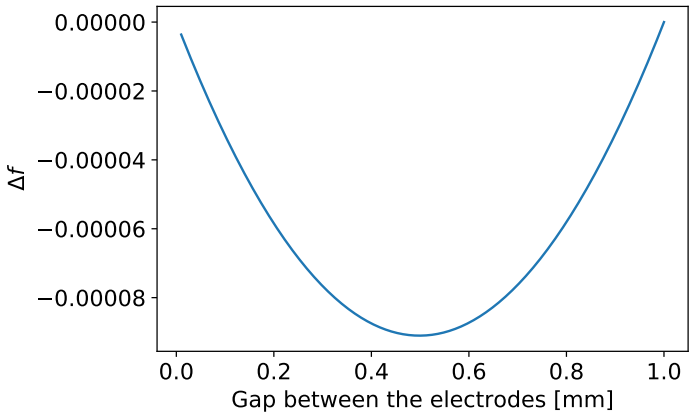


Figure 5: The difference between the actual behaviour of the field enhancement factor and a straight line connecting the values of 0.1 mm and 1 mm. The deviation between them is below 0.1‰.

For the used distances to measure data, the values of the FEF are given in Table 3:

Table 3: Values of the FEF for the distances used.

| distance [mm] | 0.05 | 0.10 | 0.15 | 0.20 | 0.25 |
|---|---|---|---|---|---|
| FEF | 1.0017 | 1.0033 | 1.0050 | 1.0067 | 1.0084 |
| distance [mm] | 0.30 | 0.40 | 0.50 | 0.75 | 1.00 |
| FEF | 1.0100 | 1.0134 | 1.0168 | 1.0252 | 1.0337 |

To calculate the electric field between two electrodes one also needs the voltage between them. The maximum voltage in vacuum where the field is stable can be described by equation 34 [18]:

$$\mathrm{U}_{\mathrm{max}} = a \cdot d^{b}. \tag{34}$$

The variables $a$ and $b$ depend on material and shape of the electrode with the restriction for $b$ that $0.4 < b < 0.7$ has to hold.
Once the voltage difference between the electrodes crosses $\mathrm{U}_{\mathrm{max}}$, the field is too high and there will be a dark current between the electrodes. This limits the field strength and is mainly caused by ionization effects on the electrodes' surfaces. As an ideal surface of the electrodes can not be reached in reality, all electrode surfaces have small irregularities. These irregularities can be minimized by different polishing techniques and coating but not completely removed. Therefore each surface has small tips, which can be approximated to have a spherical end with a radius $r_{\mathrm{tip}}$. At the end of the tips, the electric field strength is not given by the applied voltage $U$ and the distance $d$ to the other electrode, but by the voltage and the radius of the end of the tip [19]:

$$E_{\mathrm{tip}} = \frac{U}{r_{\mathrm{tip}}} \tag{35}$$

As the tips on the surface have radii in the order of micro meters and below, the electric field at their end is much higher than on average between the electrodes. This high fields cause two main effects. The first of these effects is the field emission. Caused by the high field single electrons in the electrode's surface have enough energy to tunnel the surface and

leave the electrode. These electrons can travel to the other electrode and cause a dark current between the two electrodes. As this effect mainly occurs on negatively charged electrodes, this does not play a major role during the measurements for this thesis as one electrode is grounded and the other electrode is connected to a positive charge (c.f. Section 3.2 for more details about the experimental setup.).
The other effect taking place is the ionization of rest gas particles in the vacuum. Even at a vacuum of $p = 10^{-10}$ mbar, which was typically used during the experiment, the amount of particles in the rest gas is in the order of $n = 10^6$ particles per cubic centimetre. The high fields at the end of the tips enable the ionization of single rest gas particles. The free electrons and also the charged ions are accelerated in the electric field and travel to the electrodes, which causes a measurable dark current.
Any particle with charge $q$ between the electrodes sees the electric field strength $\vec{E}$ and gets accelerated to the kinetic energy

$$T = q \cdot E = q \cdot U/d, \tag{36}$$

where $d$ is the distance between the electrodes with a potential difference $U$. With increasing distance between the electrodes, also the potential difference and the energy of the electrons and ions increases. These higher energies cause secondary ionization effects which again increase the dark current. At some point, the energy is too high and a single ionized atom will start an avalanche of ionization processes between the electrodes. This avalanche can cause a spark between the electrodes and will lead to a break down of the electric field. Additionally, this avalanche produces a larger amount of particles hitting the electrodes' surfaces. Therefore it is desirable that the electrodes do not produce any sparks, as this can cause severe damage.
According to equation 32 larger distances need larger voltages to produce the same field strength. As the maximum voltage grows slower than linear with distance, this also means that the maximum achievable field goes down with distance.
While a spark can cause critical damage, minor dark currents are likely to have no impact on the surface. Still it is desired to operate the electrodes in a region, where there is almost no dark current to minimize the risk of damage. This is even more important for electric bending elements in a particle accelerator which can not be changed easily if they are damaged.

# 3 The test setup

This chapter deals with the electrode pairs that are used for the measurements in this thesis. Additionally the experimental setup is explained and an explanation of the measurement procedure is given.

## 3.1 The four electrode pairs

The core of the setup are the four different electrode pairs. All electrodes have the shape of a half sphere with a radius of $r = 10\,\text{mm}$. Two pairs of aluminium and two pairs of stainless steel electrodes were manufactured in the workshop at Zentralinstitut für Engineering, Elektronik und Analytik[3] (ZEA) and mechanically polished. To improve the surface quality one pair of each material was coated with titanium nitride (TiN)[4]. The coating with TiN has two main advantages. TiN is much harder than stainless steel or aluminium, therefore the coating protects the electrodes' surfaces from scratches. Additionally measurements from another working group have shown, that a TiN coating on electrodes increases the maximum field strength that can be achieved [20].
Pictures of the four different electrodes are shown in Figures 6 and 7.

Figure 6: Stainless steel electrodes inside the chamber. The gap between them is 0.5 mm, their radius is 10 mm.

After manufacturing all electrodes are cleaned for ultra high vacuum (UHV) purposes. Therefore the electrodes undergo a pickling treatment and afterwards are cleaned in an ultrasonic ethanol bath to remove any substance left on the surface. Additionally each pair of electrodes is cleaned with UHV wipes and ethanol before the electrodes are installed in the vacuum chamber, to prevent the influence of any contamination on the surface which might

[3] engl: Central Institute for Engineering, Electronics and Analytics

[4] To make sure the coating is put on pure aluminium and not aluminium oxide, the aluminium electrodes were additionally laser polished directly before the coating. This removes a possible aluminium oxide layer on the surface and the coating is put directly on aluminium.

Figure 7: Three of the four different electrode types, all with a radius of 10 mm. From left to right: Coated stainless steel, aluminium and coated aluminium.

have added after the cleaning process.
The surface of all electrodes is measured at the beginning of this thesis by ZEA, to determine the roughness. These measurements are done with a white light interferometer, which has a lateral resolution of 50 nm and a height resolution of 3 nm [21]. The measured values are shown in Table 4 [22].

Table 4: Surface roughness of the different electrodes.

| first electrode | Al | ss | AlTiN | ssTiN |
|---|---|---|---|---|
| average [$\mu m$] | 0.13 | 0.10 | 0.08 | 0.08 |
| maximum [$\mu m$] | 1.11 | 0.87 | 0.95 | 1.51 |
| second electrode | Al | ss | AlTiN | ssTiN |
| average [$\mu m$] | 0.18 | 0.10 | 0.08 | 0.10 |
| maximum [$\mu m$] | 1.11 | 1.17 | 1.78 | 2.54 |

The average roughness of the surface is defined as the arithmetic mean of the absolute values of the deviation of the height from the mean height. The maximum roughness is defined as the maximum distance between the highest and the lowest point on the measured surface. Although this would also allow that there are larger plateaus or holes on the surface, the height profiles obtained during the measurements show, that this maximum roughness is caused by single tips on the surface. These tips have a width in the order of the lateral resolution, which is 50 nm.
These roughnesses are measured before the electrodes are used for the measurements in this thesis. It is possible that the roughness is larger by now, as the dark current during the measurements, as well as the mechanical stress during the measurement procedure (c.f. section 3.3) will have decreased the surface quality by now.
It can be seen, that the average roughness of the electrodes is similar for all eight measurements, although the roughness of the uncoated electrodes is a bit higher for both materials. On the other hand it can be seen that for all but one measurement the maximum roughness of the coated electrodes is larger than for the uncoated counterparts. While the uncoated aluminium electrodes both have a maximum roughness of 1.11 $\mu$m, the coated ones have a roughness of 0.95 $\mu$m and 1.78 $\mu$m. For the stainless steel electrodes, this is even more significant where a roughness of 0.87 $\mu$m and 1.17 $\mu$m of the uncoated electrodes compares to a roughness of 1.51 $\mu$m and 2.54 $\mu$m of the coated electrodes. As explained in section 2.4 these small tips create locally strong fields and therefore are a source of breakdown. For small distances, this effect will be more significant, while for larger distances, these single tips are not as important and the average roughness will dominate. Looking at the measured roughnesses

it becomes clear, that the coated electrodes have the higher maximum roughness compared to the uncoated electrodes. This could play a role for the measurements and decrease the maximum achievable fields for the electrodes.
The uncoated stainless steel and the coated aluminium electrodes were already used for measurements with the same setup before the roughness was determined. As the measurement of the roughness shows that the coated electrodes have a larger maximum roughness than the uncoated ones, now measurements shall be done for all four electrode pairs. This includes the already measured electrodes as the surface might have been different at the previous measurements and changed over time due to dark current and breakdowns. Additionally this allows to get data for all materials in similar conditions as the measurements are done by a single person.

## 3.2 The experimental environment

As mentioned before, two of the different electrodes were already used in previous measurements [23]. The setup that was used in the previous measurements is used again now. This setup uses small scale electrodes instead of real scale electrodes, which will be sufficient for first measurement results. It was decided to use a small setup because it reduces the costs and therefore allows to produce and test electrodes made of different materials. The small scale setup also allows to use standard vacuum parts, like copper sealings, which also reduces costs. Additionally, the support structures around the electrodes can be designed easier and do not have to be as strong as for larger electrodes. This allows to use the electrical feedtroughs as the mechanical supports. As a last point the small setup also means smaller gaps between the electrodes. Therefore smaller voltages are needed which means a less powerful power supply. Additionally these small voltages mean less radiation and therefore no shielding is necessary. This allows to stand next to the experiment and do the experiment in place instead of via remote control. If the voltage was higher, this would be the case for radiation protection reasons.
A picture of the whole setup is shown in Figure 8.

Inside the vacuum chamber, the electrodes are each fixed on a mounting that acts as an electrical feedtrough and as mechanical support. While the position of the lower electrode is fixed, the position of the upper electrode can be changed. This is done by a linear drive [24] (component 1 in Figure 3) with 0.01 mm scaling to vary the gap between the electrodes. The mountings both are connected to vacuum feedtroughs and outside the vacuum chamber to the electric circuit. A diagram of this circuit is shown in Figure 9.

Numerical simulations were done before building the setup. They have shown that in terms of field homogeneity there is no difference if one electrode is put on a potential of $+V_0$ while the other electrode is put on $-V_0$ or if one electrode was grounded and the other electrode was at $+2V_0$ [23]. Therefore it was decided that only one power supply is used and only the upper electrode has a potential not equal to ground. This option makes it easier to set the electric field since only one power supply has to be used and on the same time noise effects are decreased. The used power supply (component 2 in Figure 3) can deliver up to 30 kV, with a displayed step size of 100 V. The ripple is given to be below 0.01% at 30 kV [25].
To reduce the current in case of a high voltage (HV) breakdown between the electrodes, a 100 MΩ resistor is placed between the power supply and the upper electrode. The picoamperemeter (PAM) [26] (component 3 in Figure 8) is placed between the lower electrode and the ground to measures the dark current between the electrodes. To protect the PAM from high currents, two gas discharge boxes [27] and two low leaking diodes [28] are used. The PAM is set to display the running average of 50 measurement points with a resolution of 0.1 pA.
As already mentioned, the electrodes are mounted inside a UHV chamber. To get this UHV

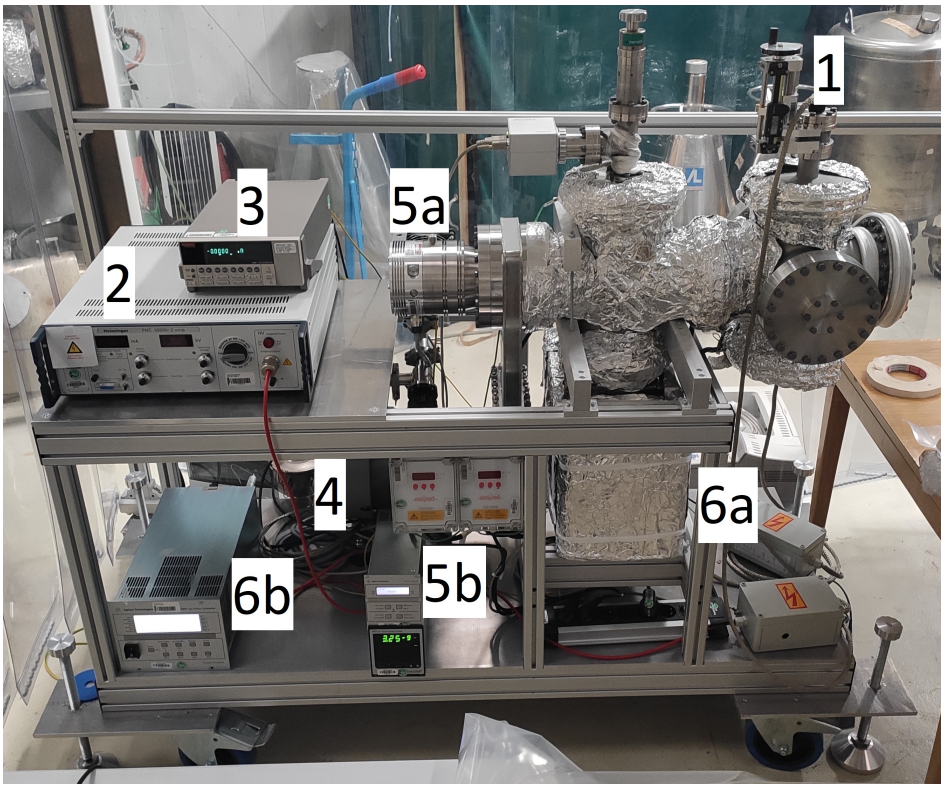


Figure 8: Picture of the setup placed in the COSY hall at the Institut für Kernphysik (engl: Institute for nuclear physics) (IKP) in Forschungszentrum Jülich (FZJ). The labelled components are: 1: linear drive, 2: power supply, 3: picoamperemeter, 4: scroll pump, 5a: turbo pump with control unit 5b, 6a: ion getter pump with control unit 6b.

a vacuum system with three pumps is needed. A scheme of it is shown in Figure 10.

The scroll pump [29] (component 4 in Figure 8) is used to decrease the pressure inside the chamber from atmospheric pressure to around $10^{-3}$ mbar. This is achieved with a pumping speed of $15\,\mathrm{m}^3/\mathrm{h}$. Once the pressure is below $10^{-1}$ mbar the turbomolecular pump [30] (component 5a in Figure 8, 5b is the control unit) is switched on. It has a pumping speed of 300 l/s and is air cooled by a fan. To get rid of humidity in the chamber, a heating device is installed outside the vacuum that heats the chamber to a temperature of up to 80° C. After baking out the chamber, the ion-getter pump (IGP) [31] (component 6a in Figure 8 with control unit 6b) is switched on and the valve [32] between the vacuum chamber and the first two pumps is closed. The IGP is mounted at the bottom of the chamber and has a pumping speed of 300 l/s. The pressure inside the chamber is controlled by the internal pressure monitor of the IGP and a further vacuum gauge at the top of the chamber. Another valve gives the option to connect the chamber with a bottle of dry nitrogen to clean the chamber after it is opened. During measurements the scroll and turbo pump are switched off to minimize vibrations. The recorded pressure by the IGP is typically in the order of $10^{-9}$ mbar.
To have a clean environment around the setup and to protect all vacuum part from dust when the vacuum chamber is opened to change the electrodes, a flowbox is used. The flowbox has an area of $12\,\mathrm{m}^2$ and is equipped with air filters of category H-14. These filters can be used to produce a cleanroom of class ISO-4 or ISO-3 when handled carefully. Since no clean room clothes are used during measurements, this limit can not be reached. A measurement of the air gives an air quality corresponding to a cleanroom class of ISO-6. Since the time where the electrodes and the vacuum chamber can be contaminated is very short this cleanroom

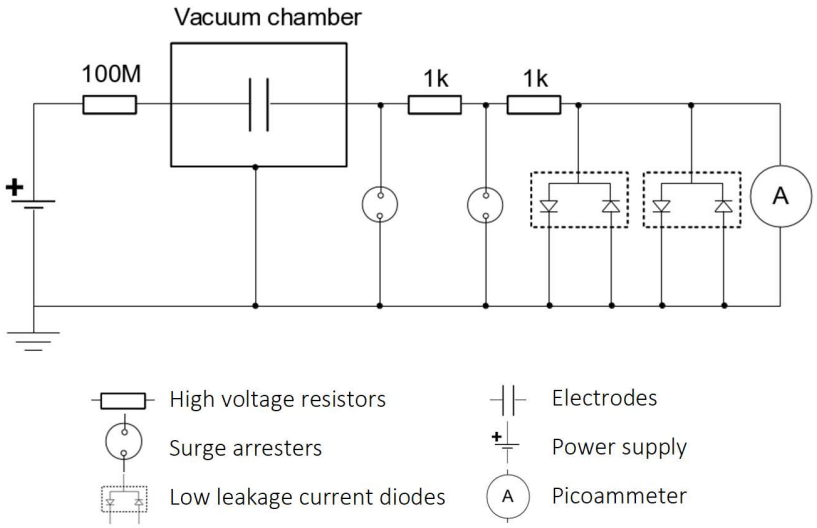


Figure 9: The electrical circuit of the setup [23].

class is still sufficient for the measurement. The flowbox including the whole experimental setup inside is placed in the COSY hall at IKP in FZJ for the measurements.

## 3.3 The measurement procedure

To measure the dark current with the setup, first the distance between the two electrodes has to be set. Since each pair of electrodes varies in their dimensions the scale on the upper electrode shows only a relative position to some random value. To get the distance between the electrodes, this scale has to be calibrated. This is done by applying a very small voltage on the upper electrode when the electrodes are not touching[5]. Afterwards, the upper electrode is lowered very carefully, while simultaneously the PAM is monitored. Once the PAM shows a current, the electrodes touch each other and the movement is stopped. This position is set to $d = 0\,\text{mm}$ on the scale. As all electrodes are slightly different in size, and also to keep possible errors caused by the scale as low as possible, this calibration is repeated before each measurement. The procedure is not ideal, as the contact between the electrodes can cause damage on the electrodes' surfaces. Still, it is the only possible option at the moment to set the distance between the electrodes and therefore the risk of damage has to be taken. After calibrating the scale, the voltage between the electrodes is switched off again.
The distance between the electrodes is always set using the same procedure to reduce the uncertainty. After the scale is set to zero, the distance is increased until it is at the desired position. If the distance shall be set to a smaller distance after the measurement, the scale is calibrated again and the distance is again set by increasing it. No measurement position is set by decreasing the distance, to minimize the uncertainty in position which might be caused by scaling effects.
Once the distance is set, the PAM is checked if the current in the circuit is zero as it should be. Then the power supply for the high voltage is switched on and the voltage is increased in steps of 500 V or steps of 200 V. The chosen size of the steps is dependent on the gap between the electrode and the already reached field. While for distances above $d = 0.2\,\text{mm}$ 500 V steps are taken, 200 V steps are used for distances with a size of 0.05 mm. For the distances between these two sizes, the measurements are started with the large voltage steps. Once the voltage becomes higher and it is expected that a current will appear within the next steps,

[5] Even when there is no scale showing the position, there is still a window to see, that both electrodes are not touching if the gap is large enough.

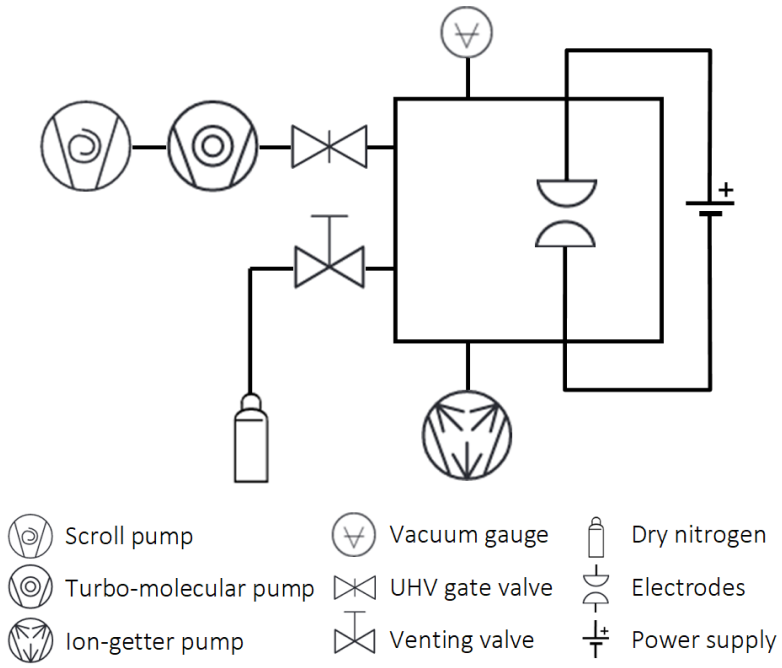


Figure 10: The vacuum circuit of the setup [23].

the step size is changed to 200 V to have a better resolution.
After each time the voltage is increased, the PAM shows a current due to the induced current caused by the voltage increase. To make sure, that the measurement results are not influenced by this, there is a pause of around ten seconds after increasing the voltage, before the dark current is read from the PAM. The PAM is monitored for about ten further seconds to get the data[6]. Since the data has to be read manually, it is not possible do get the average value of the current. Therefore the median current of this period is taken as the current while half of the distance between the largest and smallest current is taken as the uncertainty. After the data is recorded, the voltage is increased to the next value. The measurement is stopped, if one of three termination conditions is reached. These conditions are:

1. The dark current is not vanishing any more: In this case the measurement is continued with higher voltages to see the behaviour of the dark current for higher fields. The measurement is stopped when the dark current becomes larger to protect the electrodes from sparks. This stop is typically done between 300 pA and 500 pA.

2. The power supply measures a current in the circuit while the PAM does not: The power supply has an additional internal ampere meter. At higher voltages it happens that the power supply measure a current in the electric circuit, while the PAM measures no current between the electrodes. It is not clear if this is caused by the diodes or gas dischargers or if there is a real dark current between the electrode and ground which does not flow through the PAM. As a consequence, the data will most likely not give the real dark current between the electrodes. Therefore the measurement is stopped.

3. One of the electrodes sparks: High fields and impurities on the surface can cause a spark between the electrodes. If this happens, the electric circuit protects the PAM from too

[6] If the dark current showed large fluctuations or it could be seen, that the induced current from changing the voltage was still around, these ten seconds both were varied to 20 to 30 seconds.

high voltages, the power supply's internal protection switches off the voltage immediately and the measurement is stopped. Additionally, the vacuum chamber is opened and the electrodes are optically checked before they are used for further measurements.

As in all measurements, the results recorded have uncertainties that have to be considered for analysis. While measuring the dark current between the electrodes, three sources of uncertainties can influence the results:

1. The distance between the electrodes: Even if the scale is set to zero before each measurement, the scaling stays limited to a step size of 0.01 mm. The standard deviation of a uniform distribution gives
$$\sigma_d = \frac{0.01\,\mathrm{mm}}{\sqrt{12}}. \tag{37}$$

2. The set voltage: Setting the voltage in steps of 200 V or 500 V gives an uncertainty. This is especially important when the maximum voltage shall be determined where there is no dark current between the electrodes. As there are no indicators showing this is happening closer to the previous step or the next one, the uncertainty is taken from a uniform distribution and taken as the size of the voltage step divided by the square root of 12. This gives
$$\sigma_U = \frac{\Delta U}{\sqrt{12}}. \tag{38}$$

3. The measured current: The currents are read manually, by monitoring it for about ten seconds. After that the fluctuation between the maximum and the minimum of this time period is divided by two and taken as the uncertainty on the measured value. For currents around zero, this uncertainty is below 1 pA, but it increases to a relative error of around 10 % for larger currents and even around 50 % if the current is very high and the electrodes are close to sparking. Unfortunately there is no electronic readout available at the moment, so this uncertainty can not be reduced.

# 4 Measurement results

In this chapter the measurement results are shown. This is done in four parts. The first part deals with the behaviour of the dark current with increasing voltage for the different electrode pairs, in the second part measurements are done to see if the results are reproducible. After this, the maximum voltages and fields that could be achieved are discussed and compared to previous results. In the end, the measured results are extrapolated to larger distances which are similar to those that will be used in the prototype ring.

## 4.1 Behaviour of the dark current for increasing voltages

To see the different behaviour of the electrodes with rising voltage, several measurement rows are done with the different electrode pairs[7]. For each electrode pair, measurements are done at distances of up to 0.5 mm to determine the behaviour of the dark current. As an example, the recorded data of one data row is shown for each electrode pair. For each electrode pair an additional plot is shown, where the vertical axis is limited to currents below 100 pA to see more details for smaller currents. For larger distances the problem occurs that the used setup is not able to produce high enough voltages and therefore only an increase in noise could be measured but no current which is not in agreement with zero. Since they are not of interest, these measurements are not shown to keep the plots tidy. The measurements with non vanishing dark current are shown in Figures 11 to 14.

As expected, no measurement shows any current for low voltages and all measurements indicate that the point where the dark current is not vanishing any more increases with distance. Additionally for all electrodes the absolute error on the current increases with current. While equation 34 already indicates, that the maximum voltage increases with distance, the increase of fluctuation in the current is a consequence of the larger voltage differences $U$ between the electrode. Any particle with charge $q$ that is between the electrodes, such as charged ion or electrons from the rest gas in the chamber, gets accelerated up to a kinetic energy of $E_{kin} = q \cdot U$. With increasing voltage, the particles therefore have more energy and are able to produce secondary ionization effects on the electrodes' surfaces.
Figure 11 displays a smooth increase of current for most distances for the aluminium electrodes. Only for distances of 0.2 and 0.05 mm larger fluctuations can be seen. The coated aluminium electrodes (c.f. Figure 13) show a similar behaviour. Nevertheless, it is possible to measure a dark current for the coated electrodes up to a distance of 0.3 mm in the displayed example and even up to a distance of 0.5 mm in the other measurement rows, while it is only possible up to a distance of 0.25 mm for the uncoated pair.
The stainless steel electrodes (c.f. Figure 12) show a smooth increase in the dark current for all distances and the uncertainties of the current are much smaller than for the aluminium electrodes. The coated stainless steel electrodes (c.f. Figure 14) also show a similar behaviour. Nevertheless the datasets for a distance of 0.1 mm and 0.15 mm of the coated electrodes reveal a special behaviour at a voltage of 13 kV and 13.5 kV respectively. After an increase of the dark current for the previous voltages, a further increasing of the voltages leads to the dark current going down again. This effect is probably caused by dust on the material surface and did not repeat in other measurements and also did not have an impact on the maximum achievable field. With the uncoated stainless steel electrodes, a non vanishing dark current can be measured until distances of 0.15 mm, the coated electrodes allow to measure a non vanishing current until distances of 0.4 mm.
All four plots indicate that until a certain point, which is dependent on the electrodes and the distance between them, no current flows. Beginning at this point, the current increases

[7] This section deals solely about the question how the dark current behaves with increasing voltage for the different electrodes on a qualitative perspective. The difference between the electrodes in a quantitative perspective are shown in section 4.3

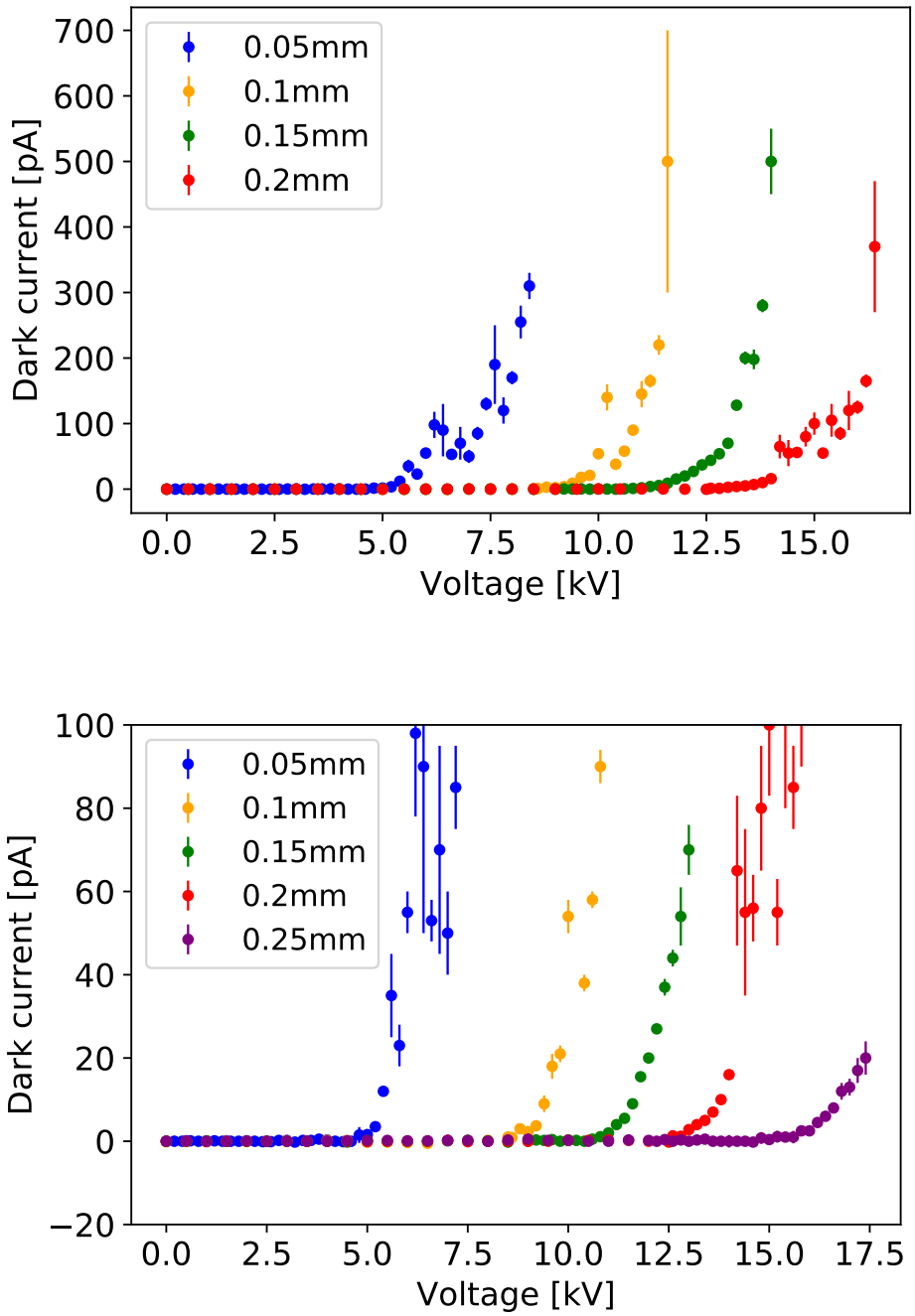


Figure 11: The measured dark current for half spherical Aluminium electrodes with a radius of $r = 10\,\text{mm}$. (up: full plot, down: vertical zoom.)

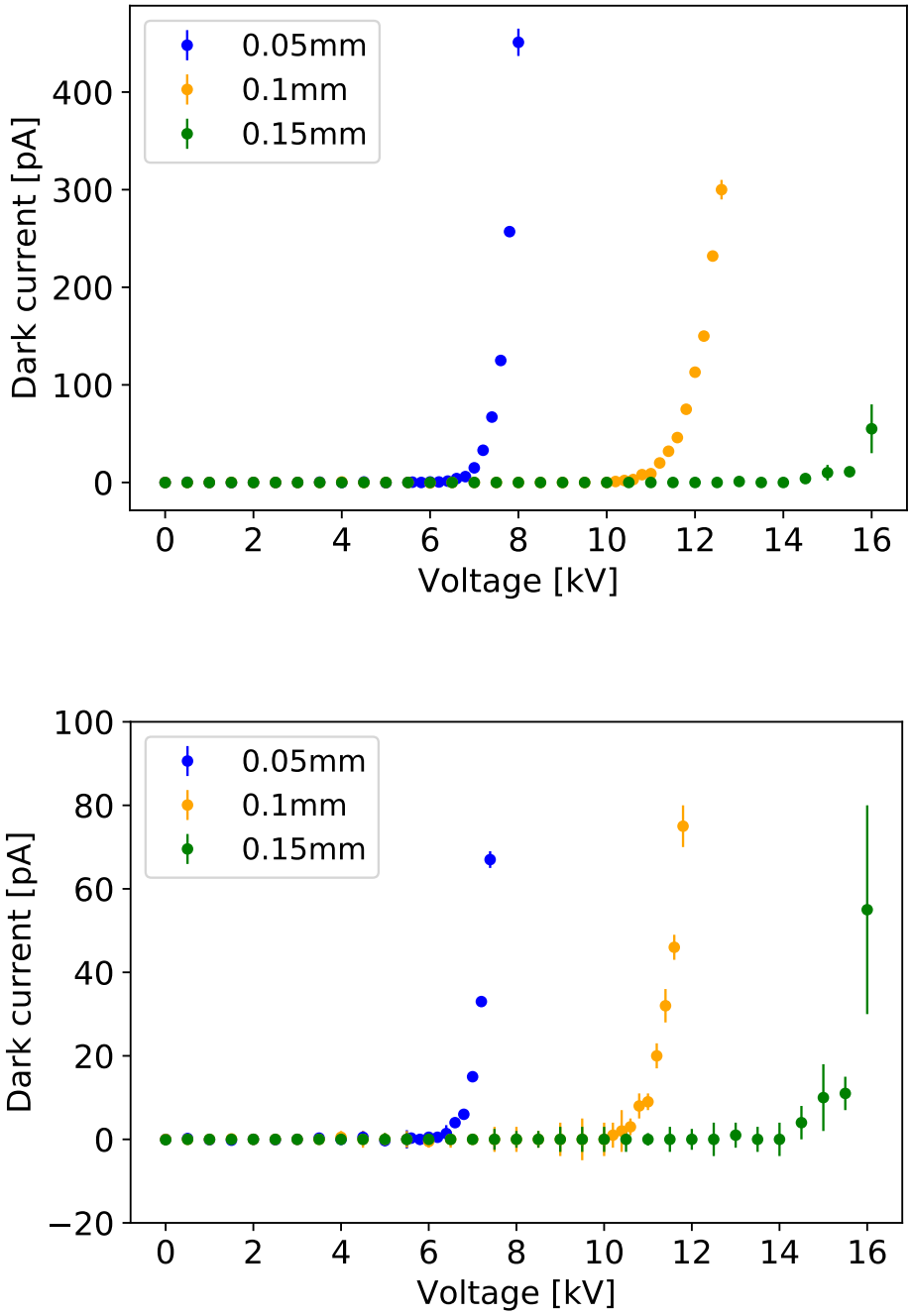


Figure 12: The measured dark current for half spherical stainless steel electrodes with a radius of $r = 10\,\text{mm}$. (up: full plot, down: vertical zoom.)

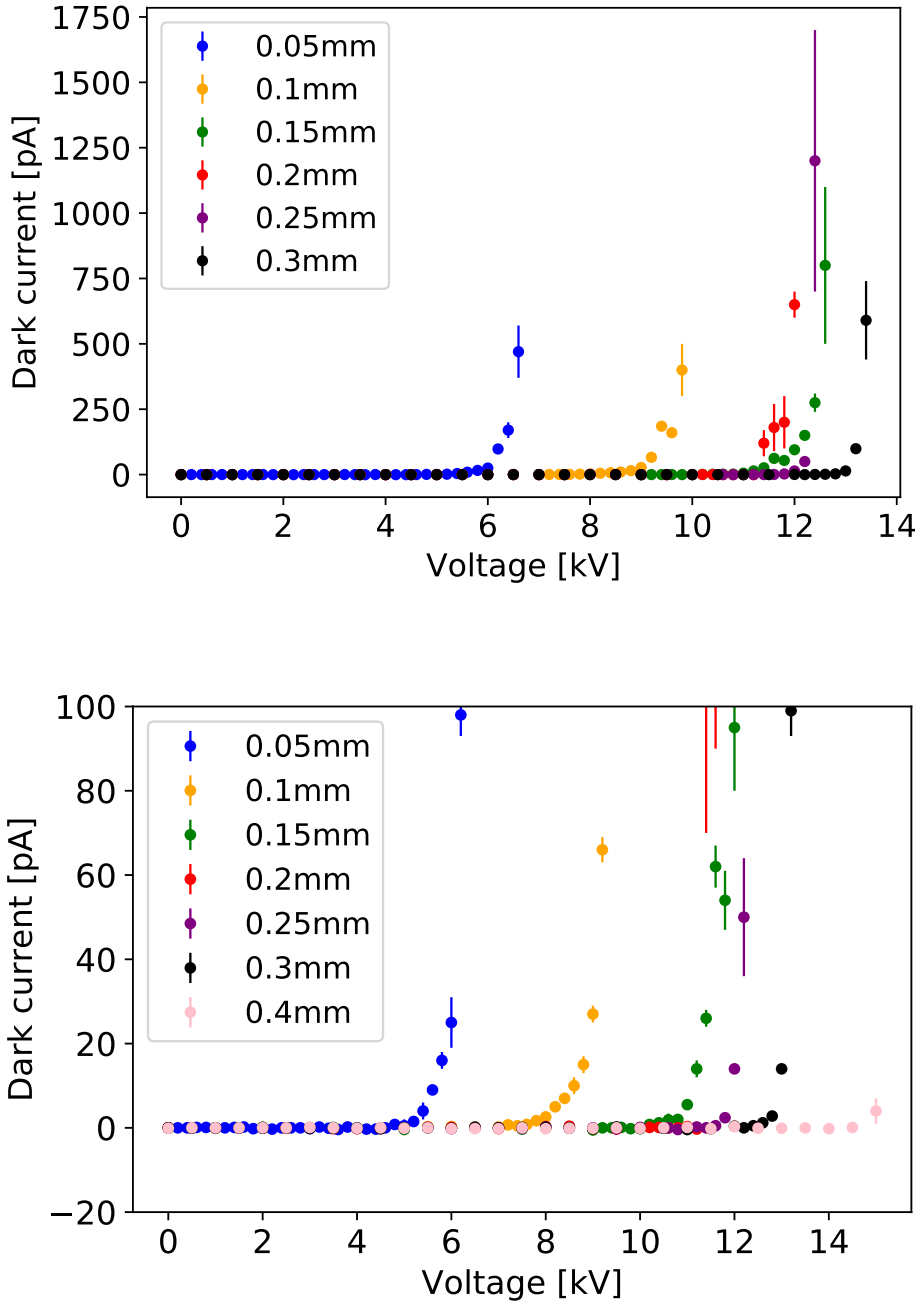


Figure 13: The measured dark current for half spherical coated Aluminium electrodes with a radius of $r = 10\,\text{mm}$. (up: full plot, down: vertical zoom.)

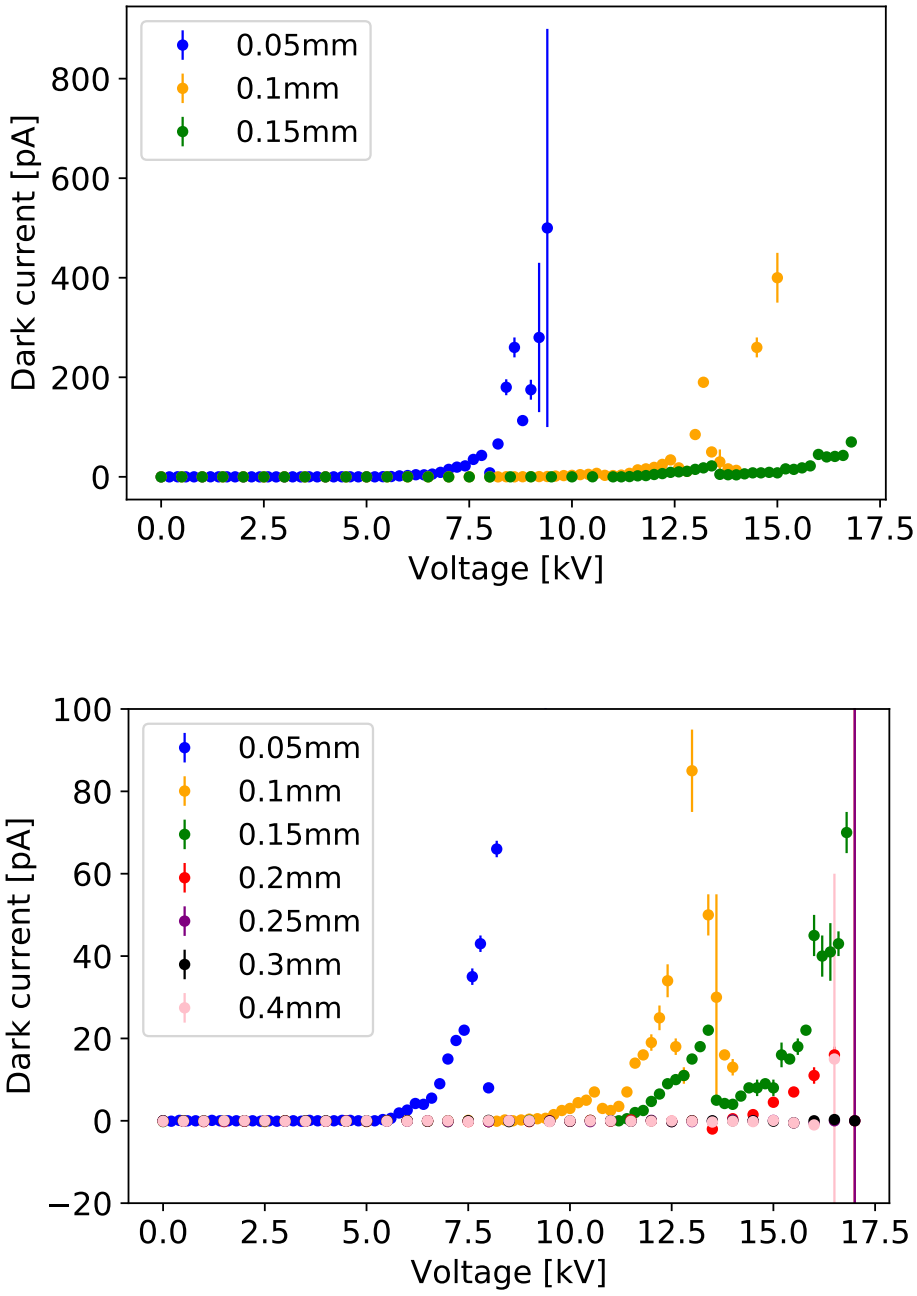


Figure 14: The measured dark current for half spherical coated stainless steel electrodes with a radius of $r = 10\,\text{mm}$ v. (up: full plot, down: vertical zoom.)

with an exponential shape for all measurement rows. This means that there is no difference in the behaviour of the dark current for the different electrodes.
While these results do not reveal any significant difference between the behaviour of the dark current for the different electrodes, they already indicate that the different electrodes can produce different field strengths before they produce a dark current. In a particle accelerator the electric bending elements shall be operated at almost no dark current. Therefore it is more of interest which field strengths are achievable with the different electrodes than how the dark current behaves if the field is too strong. Therefore the further analysis focuses on the question which field strength is achievable with which electrode type.

## 4.2 Reproducibility of the results

To find out, which electrodes are best in terms of a high field stability, for each dataset the maximum voltage is determined at which the dark current is in agreement with zero. The current is considered being in agreement with zero if $I \pm \sigma_I$ includes 0. This voltage is then taken as the maximum voltage before a breakdown for each pair of electrodes. To see how reproducible the measurement results are, two measurement rows are done with aluminium electrodes. These rows are measured at an electrode distance of 0.10 mm and 0.25 mm. To also test the reproducibility of positioning the upper electrode, these two rows are done simultaneously. Therefore, the upper electrode has to be repositioned before each measurement and the results do not only show how the data fluctuates but also how reproducible the setting of the distance is. Figures 15 and 16 show the maximum voltages that could be applied in both measurement rows. While the x-axis gives the numbers of the measurements, the figures also include the weighted means and indicate the area that is within a one sigma uncertainty.

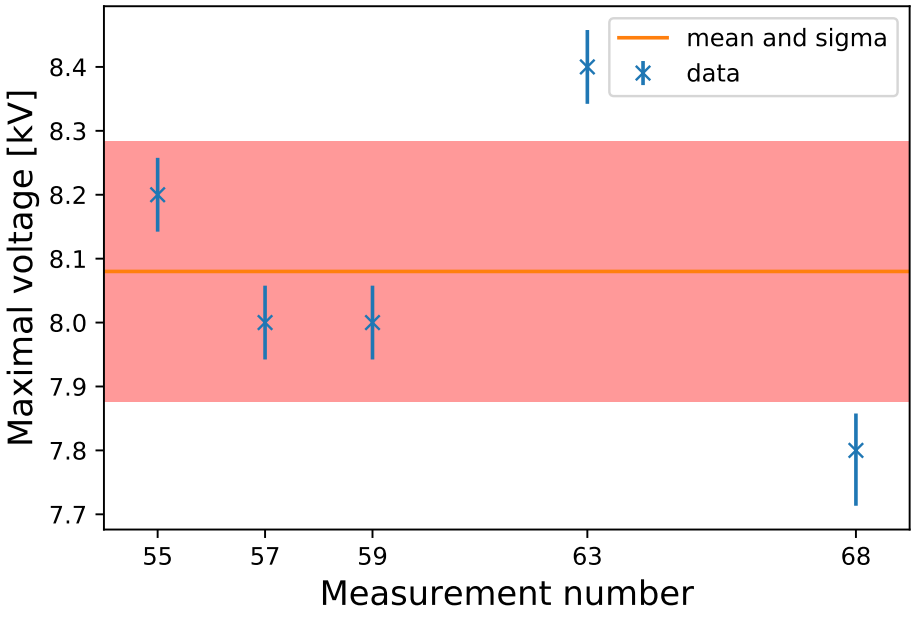


Figure 15: The maximum voltages for the first measurement row at $d = 0.10\,\text{mm}$. Also plotted is the one sigma area around the weighted mean. The data point for measurement number 68 has an asymmetric error due to a change of the voltage step size at the point of maximum field. Measurement number 61 is not analysed because after measuring an error in the data was noticed. Additionally measurement 68 is used, which belongs to the first measurement row to determine the maximum field strength (c.f. section 4.3).

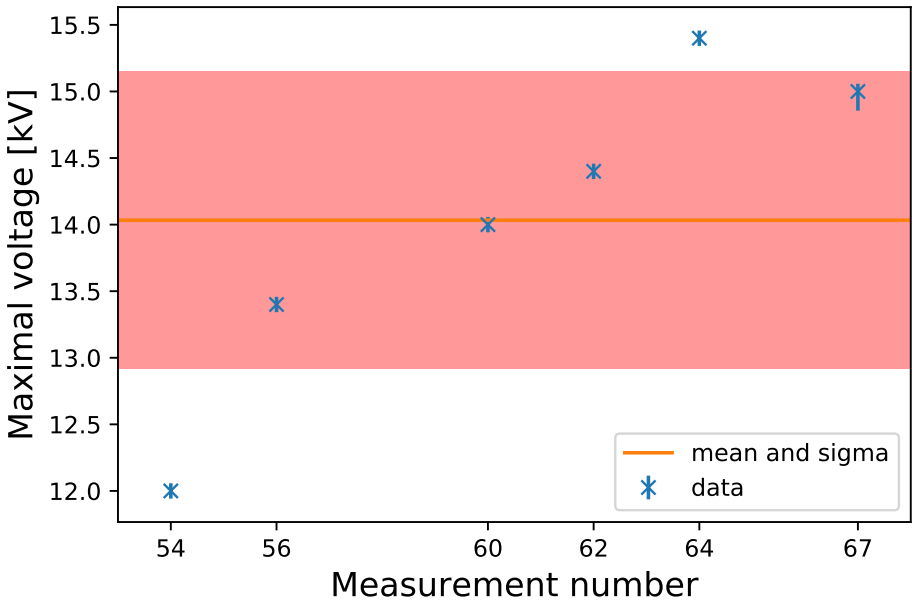


Figure 16: The maximum voltages for the second measurement row at $d = 0.25\,\text{mm}$. Also plotted is the one sigma area around the weighted mean. The size of the individual errors is similar to Figure 15, they just look smaller due to the different scale for the y-axis. The data point for measurement number 67 has an asymmetric error due to a change of the voltage step size at the point of maximum field. Measurement number 58 is not analysed because after measuring it was noticed that the position was set wrong. Additionally measurement 67 is used, which belongs to the first measurement row to determine the maximum field strength (c.f. section 4.3).

Measurement row one shows fluctuations between the maximum voltages of 0.6 kV with a weighted mean of $8.08 \pm 0.20\,\text{kV}$. Additionally no general trend to higher or lower voltages can be seen over the measurements.
The fluctuations in measurement row two are larger and include an area of 3.5 kV. This larger fluctuation can also be seen in the larger uncertainty on the weighted mean of $14.0 \pm 1.1\,\text{kV}$. Additionally a general trend can be seen. The maximum voltage increases for all but the last steps, while it showed a fluctuation in the first measurement row. This increase of maximum voltage can not be caused by a conditioning effect of the electrodes. If it was caused by conditioning, measurement row one would show the same increase as it is measured at the same time, but it does not show it.
To get more information about the reproducibility, especially under the light that the two measurement rows give different results, a third measurement row is done. This row is measured at a distance of 0.10 mm, which is the same as for measurement row one, to see if the increasing of the maximum voltage can also be detected for the smaller distance. Additionally the position of the upper electrode is not changed during this data row. Therefore this measurement row also tests, if the fluctuations in the first two measurement rows are maybe caused by a wrong positioning of the upper electrode. The results of the third measurement row are shown in Figure 17.

The fluctuations in this data row are in an area of 0.8 kV. The weighted mean of this data is given by $8.46 \pm 0.24\,\text{kV}$ and the data does not show any systematics around the value only statistical fluctuations.
To compare the values of all measurement rows, Table 5 lists the weighted means of all measurement rows.

It can be seen that the fluctuation in the data in the first and third data row are of similar

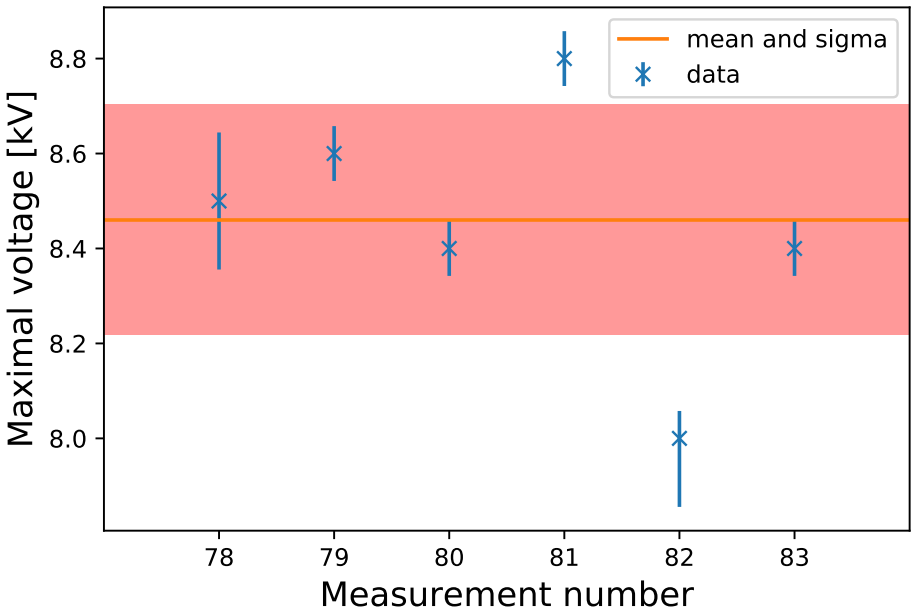


Figure 17: Maximum voltages for the third measurement row at $d = 0.10\,\text{mm}$. Also shown is the one sigma area around the weighted mean.

Table 5: Mean voltages of the reproducibility measurements.

| Data row | 1 | 2 | 3 |
|---|---|---|---|
| gap [mm] | 0.1 | 0.25 | 0.1 |
| maximum fluctuation [kV] | 0.6 | 3.5 | 0.8 |
| $U_{mean}$ [kV] | 8.08±0.20 | 14.0±1.1 | 8.46±0.24 |

size, while row two shows fluctuations larger by a factor of five. This factor can also be seen in the uncertainty on the mean. Additionally it can be seen that the weighted mean of data rows one and three are in agreement, although measurement row one included repositioning of the upper electrode while measurement row three does not. This shows that the positioning of the electrode does not significantly increase the uncertainty if done properly. The comparison between these two rows also shows, that no general conditioning of the electrodes is taking place. The electrodes were placed under vacuum conditions the whole time between the measurements and an additional amount of nine data rows for further measurements were taken. Nevertheless the third data row shows similar results as the first row whereas conditioning would lead to significant better results.
It is unclear where the increase in voltage comes from. Previous measurements with this setup did not show any effect like measurement row two [33]. A look in the measured raw data, including the pressure inside the vacuum chamber, does not show any significant difference between the measurements, except the different maximum voltage. As it is not clear why this behaviour is present, further measurements must be done to get more information and see if the effect of increasing maximum voltage still appears.
Since data row two is the only of the three rows measured which shows this increase and also previous results did not show it, it is assumed that the maximum voltage for a fixed distance with the same electrode is reproducible.
The smallest uncertainty on the mean value is $\sigma = 200\,\text{V}$ from measurement row one. The uncertainty caused by the size of the voltage steps during the measurements is either $\sigma = 200\,\text{V}/\sqrt{12} \approx 58\,\text{V}$ or $\sigma = 500\,\text{V}/\sqrt{12} \approx 144\,\text{V}$, which is significantly smaller. In section

4.3 the maximum field strength for each electrode is determined. If possible, multiple measurements are done for each point to get a sufficient amount of statistics. In case it is not possible to get enough statistics, the uncertainty on the measured maximum voltage is always taken to be at least 200 V, which is the minimum fluctuation during the reproducibility measurement.
As the measurements show that the results are reproducible, results taken over several weeks can be compared[8], which is needed for the next part of measurement and analysis.

## 4.3 Maximum field strengths for different electrodes

To determine the quality of the different electrodes, measurements to determine the maximum achievable field strength are done with all four different electrodes pairs. For these measurements the procedure is the same as the procedure that was used to check the reproducibility of the measurement. First test measurements, that were used to get to know the experimental setup and procedure showed, that almost all measurements for a distance larger than 0.5 mm have to be stopped because of a current measured by the power supply. Therefore only measurements up to a distance of 0.5 mm are done.
To get a sufficient amount of statistics, the measurements are repeated three to five times for the different electrodes. During the measurement the problem occurred that the power supply measured an internal current beginning at a voltage around 15 kV. Because of this, the maximum field up to a distance of 0.5 mm could only be measured for the coated aluminium electrodes. For uncoated aluminium, coated stainless steel and uncoated stainless steel the maximum voltage could be determined up to a distance of 0.25 mm, 0.20 mm and 0.15 mm respectively. This problem also caused, that for a small amount of combination of distance and electrode type only one or two measurements could be done which results in no statistics for these points. In this case, the measured value of $\sigma = 0.2\,\text{kV}$ from the reproducibility measurement is taken as the uncertainty to make sure the uncertainty on the recorded maximum voltage is not underestimated. The results obtained are shown in Figure 18.

To compare the measured data with equation 34, an orthogonal distance regression (ODR) is done with the free parameters $a$ for the amplitude and $b$ for the exponent. The results of this regression are shown in Table 6 and in Figures 19 to 22.

Table 6: Obtained parameters for the ODR fits.

| material | a [kV] | b | $\chi^2$/ndf |
|---|---|---|---|
| Al | 33.2 ± 3.6 | 0.608 ± 0.061 | 0.36/3 |
| ss | 50.7 ± 9.2 | 0.675 ± 0.086 | 0.10/1 |
| AlTiN | 20.96 ± 0.50 | 0.427 ± 0.022 | 7.9/6 |
| ssTiN | 40.0 ± 3.6 | 0.639 ± 0.052 | 1.1/2 |

The residuals of all four plots do not show any systematics. The $\chi^2$/ndF for aluminium and stainless steel electrodes is 0.36/3 and 0.10/1 respectively which is relatively low. One reason may be that the error is overestimated, due to the large fluctuations between the measurements. The other reason may be that a function with two parameters is fitted to data sets with five or three data points. Especially for the data row with three data points it is plausible that the function describes the data so good just by chance. The $\chi^2$/ndF for the coated aluminium and coated stainless steel is 1.2 and 0.6 respectively. This shows that the fitted function is a good representation of the measured data. Additionally it can be seen, that the fitted parameter $b$ is between 0.4 and 0.7 for all fits as was demanded. This was not put into the fitting program as a condition but came out with the fit results anyhow. This

[8] As long as there is no damage on the electrodes caused by sparks or external forces in times they are not installed in the chamber.

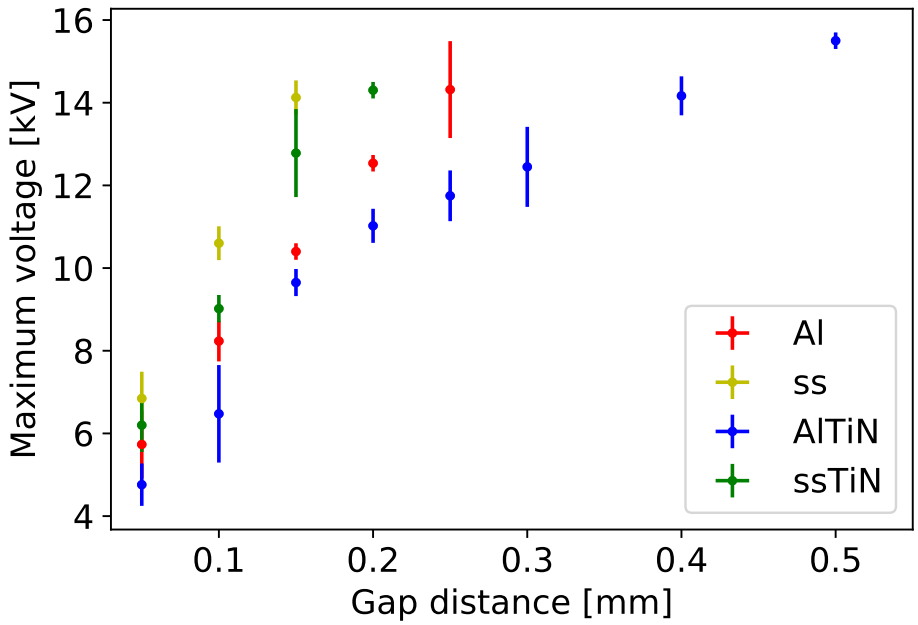


Figure 18: Maximum voltages for the different electrode pairs. The uncertainties on the position are smaller than the dot of the data point. Therefore they can not be seen.

also indicates that the data can be represented by the used function.
The value of interest for an electric bending element is not the amount of voltage between two electrodes but the electric field between them. To calculate the electrical field, equation 32 is used. The uncertainty on the field strength is obtained by Gaussian error propagation and can be described by

$$\sigma_E = \sqrt{|\frac{\partial E}{\partial U} \cdot \sigma_U|^2 + |\frac{\partial E}{\partial f} \cdot \sigma_f|^2 + |\frac{\partial E}{\partial d} \cdot \sigma_d|^2} \tag{39}$$

$$= \sqrt{|\frac{f}{d} \cdot \sigma_U|^2 + |\frac{U}{d} \cdot \sigma_f|^2 + |\frac{fU}{d^2} \cdot \sigma_d|^2}. \tag{40}$$

For the uncertainty $\sigma_f$ of the FEF, only the uncertainty on the position has to be taken into account, the uncertainty on the radius of the electrodes is small enough to be neglected:

$$\sigma_f = \perp \frac{\partial f}{\partial d}\sigma_d \perp \tag{41}$$

$$= \frac{1}{4}\left[\frac{1}{r} + \left(\sqrt{\left(1+\frac{d}{r}\right)^2 + 8}\right)^{-1} \cdot \left(\frac{1}{r} + \frac{d}{r^2}\right)\right] \cdot \sigma_d. \tag{42}$$

Figures 23 and 24 show the calculated electric field obtained by the recorded voltages. The figures also include the electric fields that will be reached if the voltage follows the just fitted functions.

All four electrode pairs are able to produce fields in the order of 100 MV/m for very small distances with stainless steel reaching the strongest field with roughly 135 MV/m. All electrodes show the same trend that the maximum field decreases with increasing distance. The errors on the electric field are larger than for on the voltages, especially for small distances. This is caused by the inverse proportionality of the electric field to the distance. Therefore

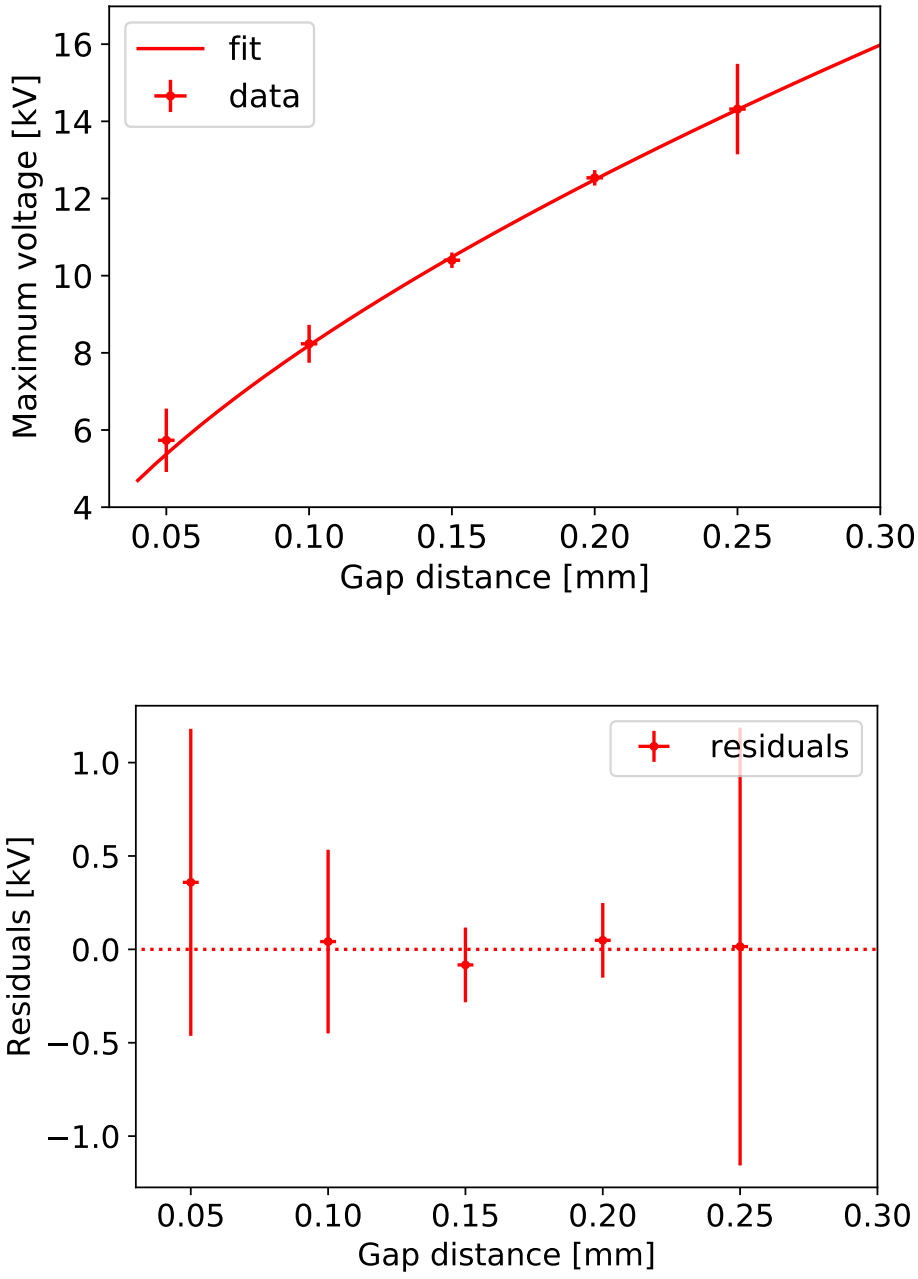


Figure 19: Measured maximum voltages for aluminium electrodes and fit according to equation 34. The bottom shows the residuals.

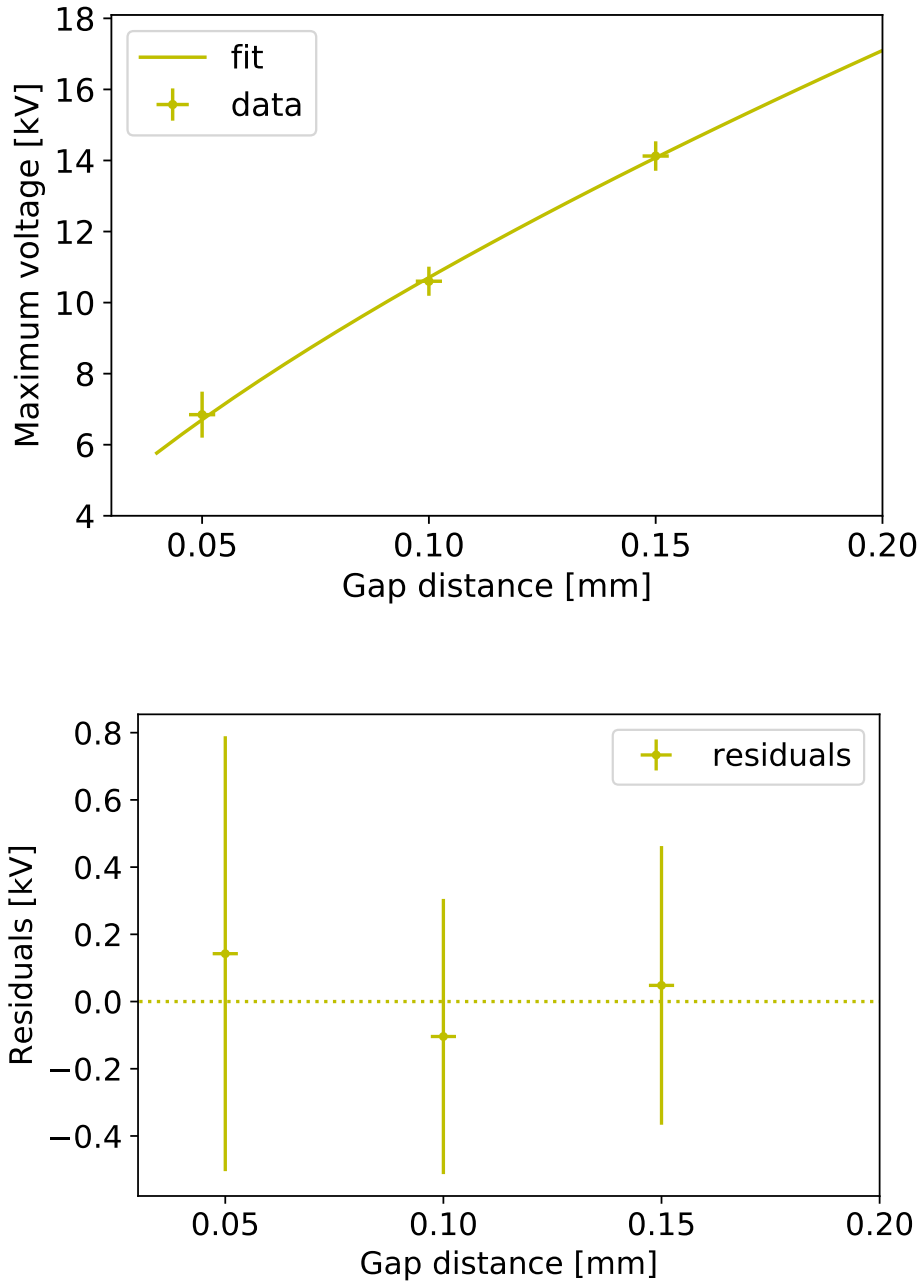


Figure 20: Measured maximum voltages for stainless steel electrodes and fit according to equation 34. The bottom shows the residuals.

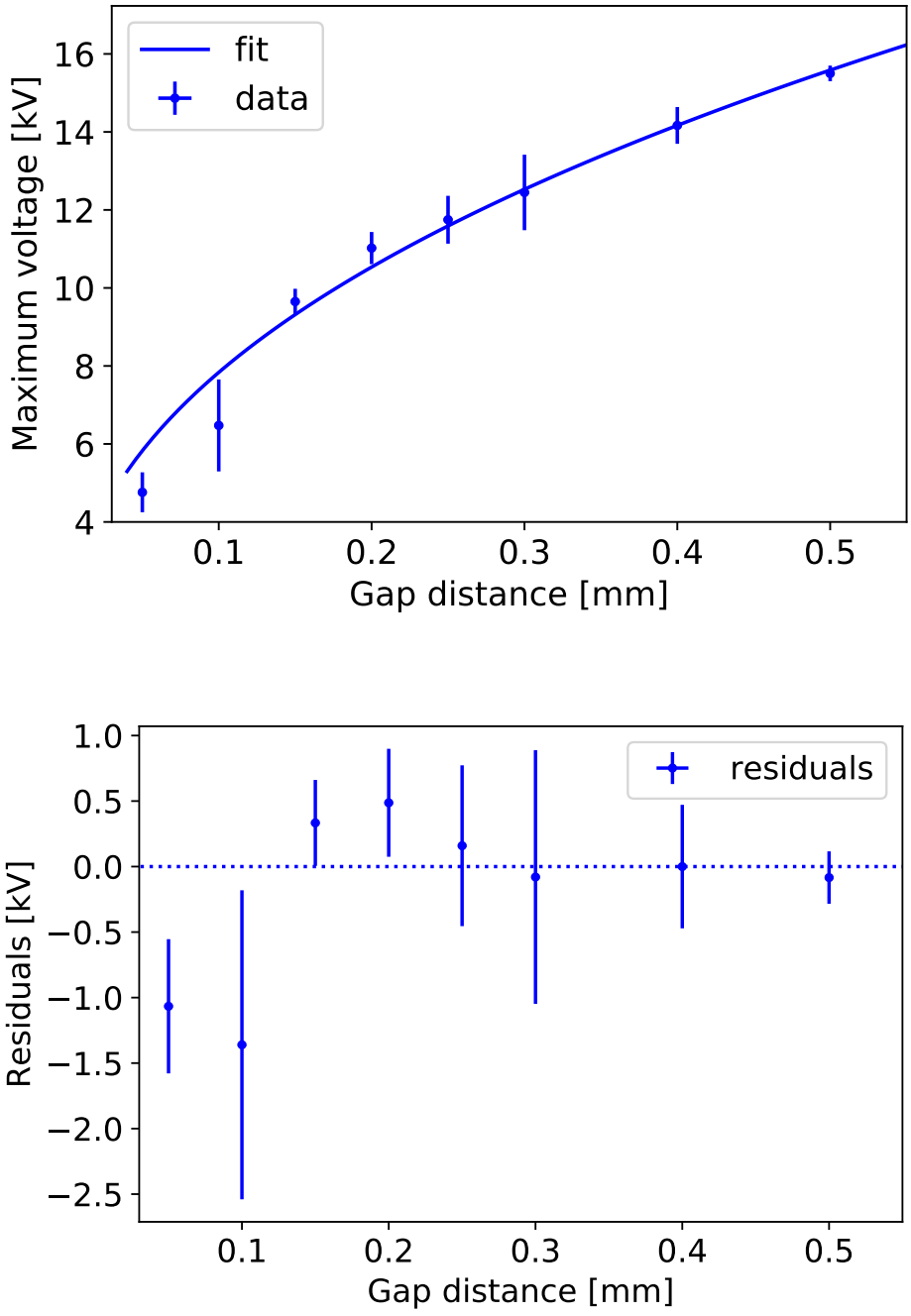


Figure 21: Measured maximum voltages for coated aluminium electrodes and fit according to equation 34. The bottom shows the residuals.

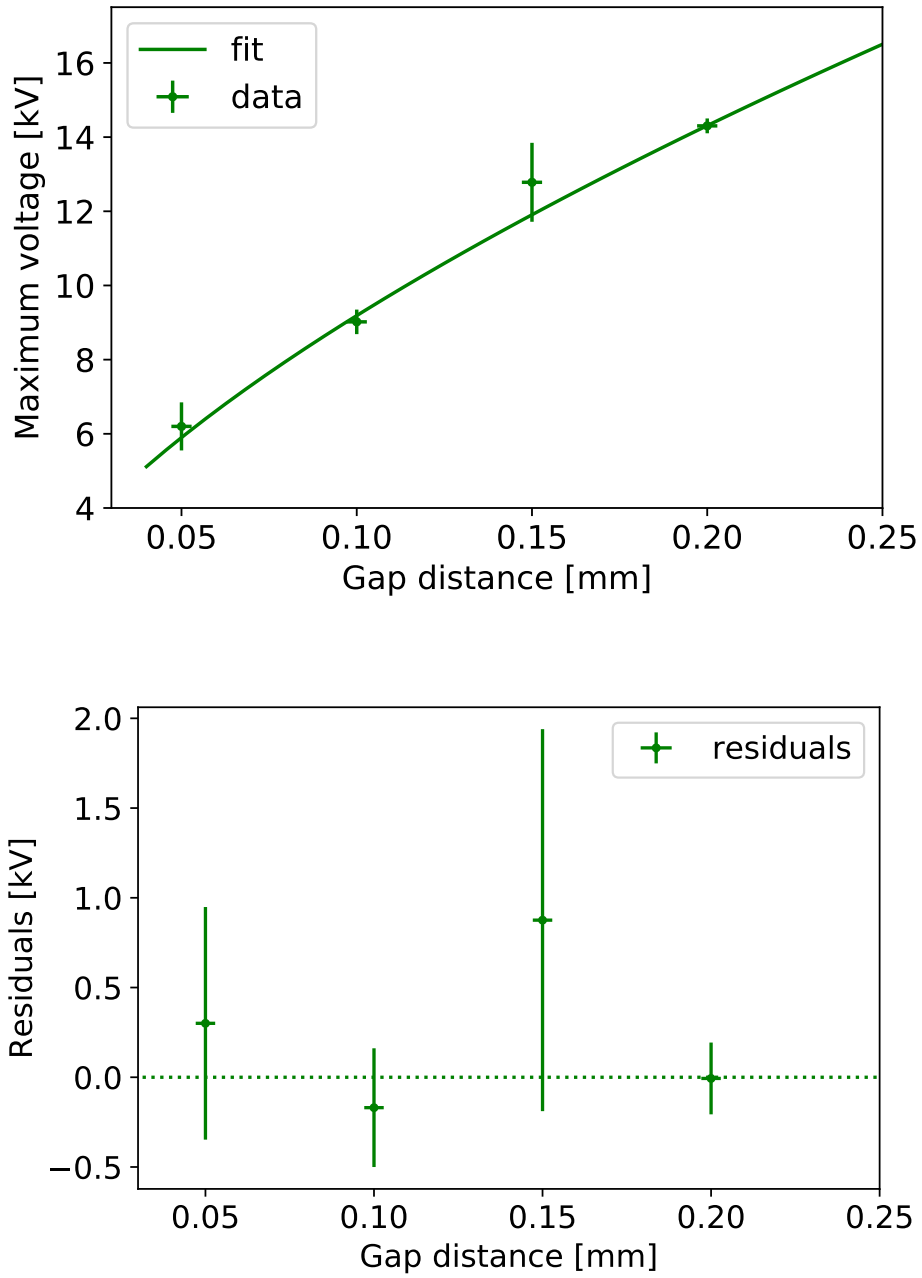


Figure 22: Measured maximum voltages for coated stainless steel electrodes and fit according to equation 34. The bottom shows the residuals.

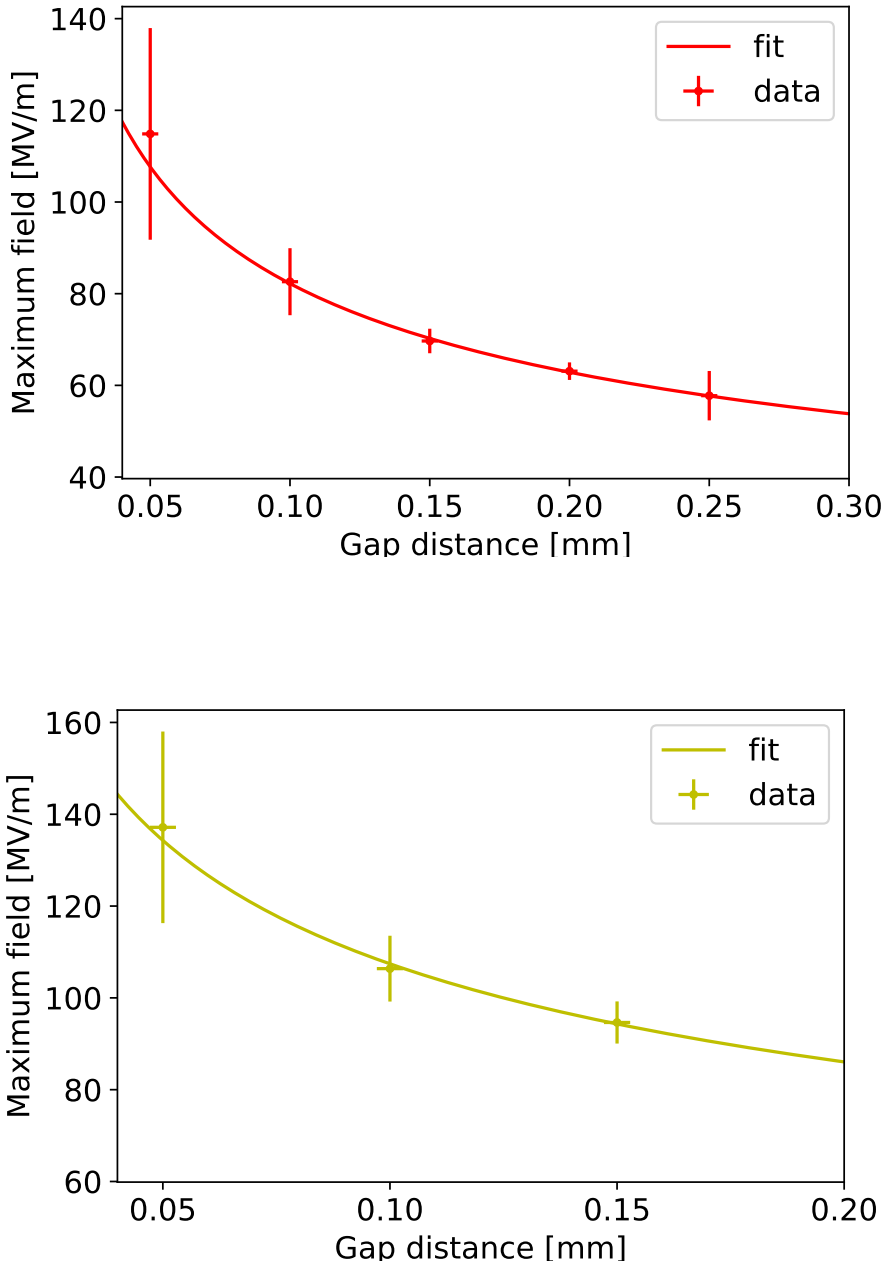


Figure 23: The maximum achieved electrical field with the recorded voltages and the theoretical field motivated by the fit. Top: Aluminium. Bottom: Stainless steel.

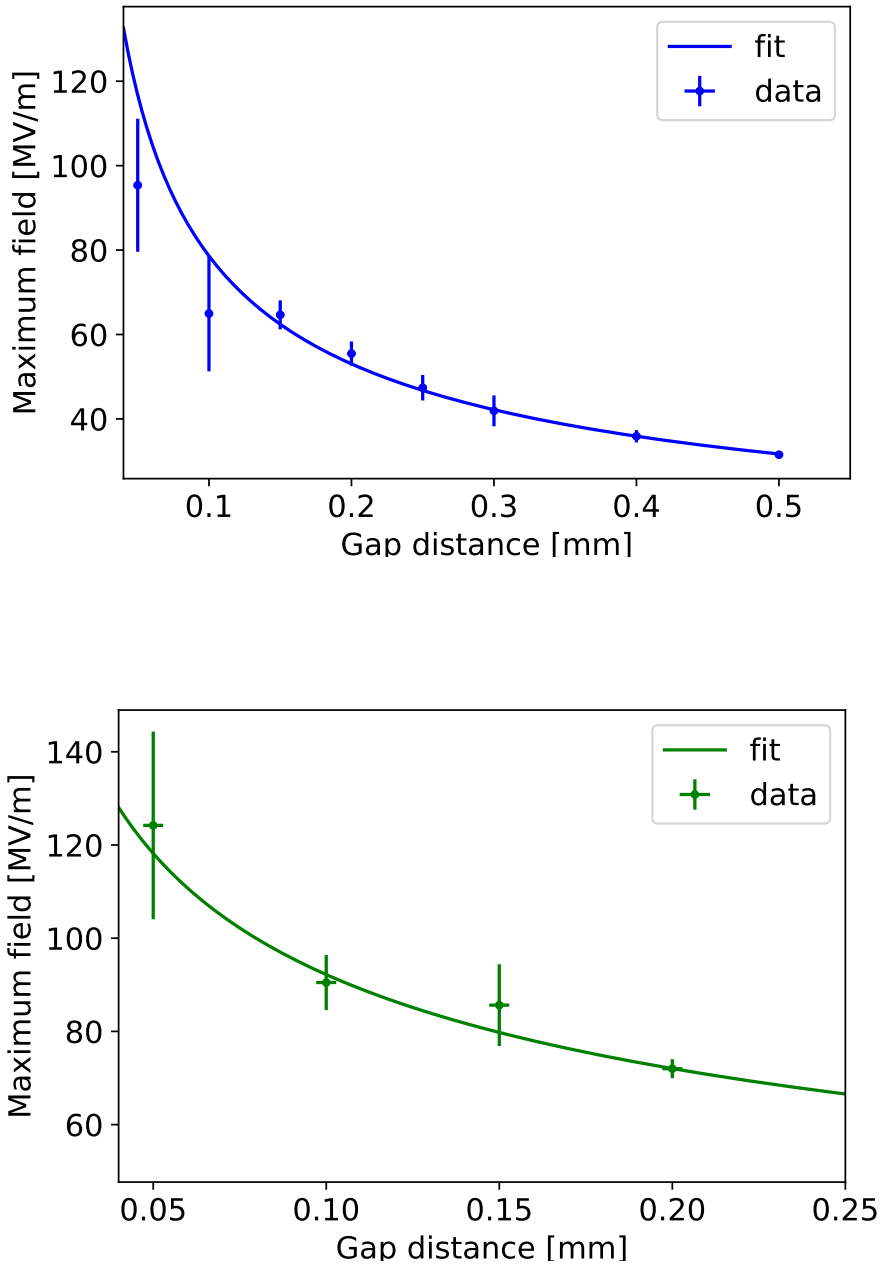


Figure 24: The maximum achieved electrical field with the recorded voltages and the theoretical field motivated by the fit. Top: Coated aluminium. Bottom: Coated stainless steel.

a small uncertainty on the distance can have a large influence on the field, especially for smaller distances where the relative error on the distance is larger. To compare the different materials, the reachable electrical field strengths as obtained with the fitted voltages are all shown in one plot in Figure 25.

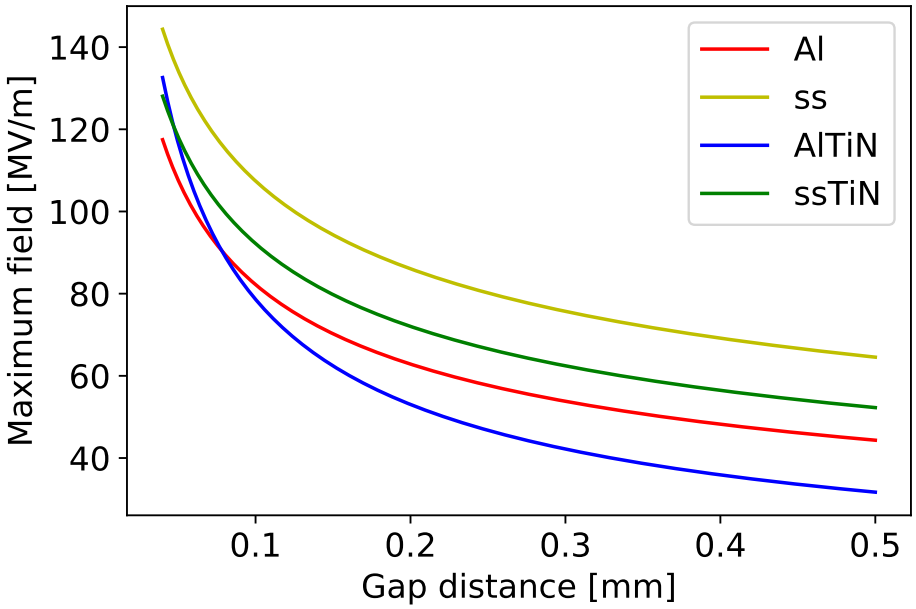


Figure 25: The maximum achievable fields as obtained from the fitted parameters in the measured range.

According to the fit, the stainless steel electrodes are able to reach the strongest stable field in the whole measured range of distance. They are followed by the coated stainless steel, aluminium and coated aluminium electrodes, except for gaps below 0.05 mm, where the coated aluminium electrodes are second best.
Additionally two systematics can be seen in the results. The first effect that can be seen is that for both materials the coated electrodes reach less field strength than the uncoated electrodes. This is contradictory to the expectation that coated electrodes can reach higher fields because of the smoother surface. As measured in Table 4, the average roughness of the coated electrodes is indeed better than the roughness of the uncoated electrode pairs, but both coated electrode pairs have a larger maximum roughness than the uncoated electrodes. This maximum roughness means that single tips are on the electrodes' surfaces. For the small distances measured the electrodes reached high field strengths, which are even stronger at the tips' ends. At these points, the field is high enough to produce ions or have field emission on the electrode surface which is sufficient for the measured dark current. Additionally, these roughnesses were measured before the measurements for this thesis. During the measurements, the surfaces might have gotten more damage caused by the dark current between them, the calibrating procedure when the electrodes touch and also if they are not handled carefully, when they are outside the vacuum chamber. Therefore the roughness can be even worse now, which is especially the case for both aluminium electrode pairs, as aluminium is much softer than stainless steel.
The other systematic that can be seen is that both pairs of stainless steel electrodes are able to produce stronger fields than both electrode pairs made out of aluminium. This can not be explained by the measured maximum roughness, as the uncoated electrodes of both materials show a similar roughness and the coated stainless steel electrodes are even worse in roughness than the coated aluminium electrodes. Therefore these results can either be caused by damage to the electrodes' surfaces after determining the roughness or that stain-

less steel electrodes are simply able to reach higher fields in the measured distance range. As the surfaces are not measured again after the experiment, this can not be completely solved.

## 4.4 Comparison with previous results

As the measured results are somehow unexpected and two of the four different electrode pairs were already used for previous measurements, the results for these two electrode pairs are now compared to see if the systematics noticed in the last chapter could already be seen before and also to see if the results match. The results of the previous measurements are taken from [33].
In a first step, the results for the both measured electrode pairs are compared. The maximum achievable field strengths obtained during these measurements are shown in Figures 26 and 27.

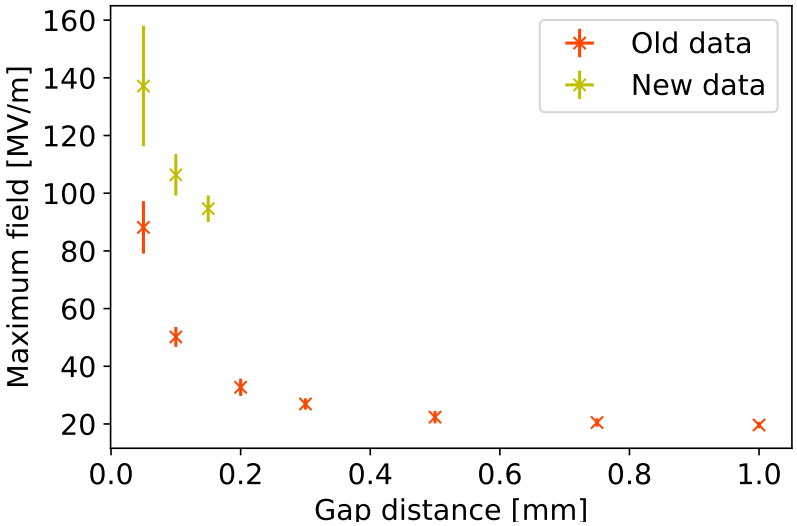


Figure 26: The maximum achievable fields for stainless steel electrodes from the previous measurements. Also shown are the new results to compare them.

Both materials show that the new results are much better at small distances than the previous results. For the stainless steel electrodes, the maximum field that could be measured for a distance of 0.05 mm now is almost 140 MV/m while previously it was about 90 MV/m, which is an increase of about 55%. For a gap of 0.10 mm the increase is even larger with 120% from 50 MV/m to 110 MV/m.
The coated aluminium electrodes show similar increases in the order of 30% to 60% for gaps between 0.05 mm and 0.30 mm. The maximum field strength for a gap of 0.5 mm is about 30 MV/m for both measurement rows.
This effect can be explained for both electrode pairs. At the beginning of the measurements for this thesis, the valves of the vacuum chamber were opened in the wrong order, when the electrodes should be changed. This led to a lot of dust being flushed inside the chamber. Before this mistake, only very small amount of dust could reach the inner side of the chamber. These amounts were not much but still it was possible to see very few dust inside the chamber, which was neglected at that point. After the mistake, a lot of dust could be seen inside the chamber and the decision was made to clean it. Therefore the whole chamber was cleaned using UHV wipes and ethanol to remove the dust. Additionally the whole chamber was flushed with nitrogen to clean regions in the chamber which could not be cleaned with

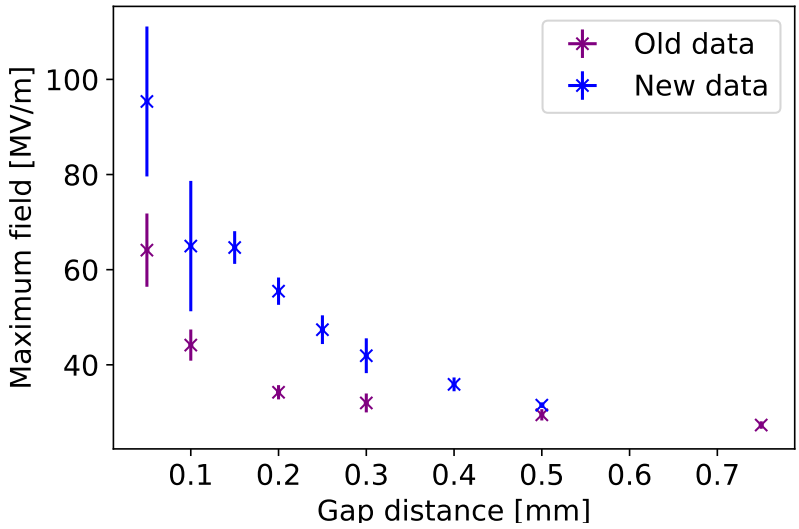


Figure 27: The maximum achievable fields for coated aluminium electrodes from the previous measurements. Also shown are the new results to compare them.

the wipes. After this process, the chamber was cleaner than before and could be used again. No dust could be seen in the chamber any more, opposite to before the contamination.
This means, that during the new measurements the chamber was cleaner than before. Therefore less particles such as dust could influence the field between the electrodes and higher fields could be reached.
The other effect that can be seen in the two figures is that the previous measurements were able to measure the maximum fields for larger distances than what was achievable with the new measurements. While for the new measurements, the maximum field can only be measured until a distance between the electrodes of 0.15 mm for the stainless steel and 0.50 mm for the coated aluminium electrodes, the previous measurements could reach this up to distances of 1.00 mm and 0.75 mm for stainless steel and coated aluminium electrodes respectively.
This effect can be seen as a consequence of the higher fields caused by the cleaner vacuum chamber. Since the fields are stronger in the new measurement, larger voltages have to be set on the power supply. Figure 28 compares the maximum voltages that were needed to reach the maximum field for the old and new measurements.

For the coated aluminium electrodes, where similar fields could be measured and also the distances achieved are comparable, the voltages show a similar magnitude. For the stainless steel electrodes stronger fields could be reached and therefore larger voltages were needed. It can be seen that the maximum voltage for the old measurements was both time around 20 kV, while for the new measurements it is both time around 15 kV. This indicates that the maximum voltage is limited by the test setup in both cases. The difference of 5 kV can be explained either by small changes to the grounding of the setup or by the fact that two different persons did the measurements. It is possible that in the previous measurements the data taking was not directly stopped when the power supply records a current which allows to use higher voltages.
The fact that the previous measurements were able to determine the maximum field for larger distances can also be used to see how the electrodes behave at larger distances. To see this, the results for both electrode pairs are plotted together in Figure 29.

Similar to the new results the stainless steel electrodes can achieve stronger fields at small gaps than the coated aluminium electrodes. At a distance of 0.20 mm the maximum fields

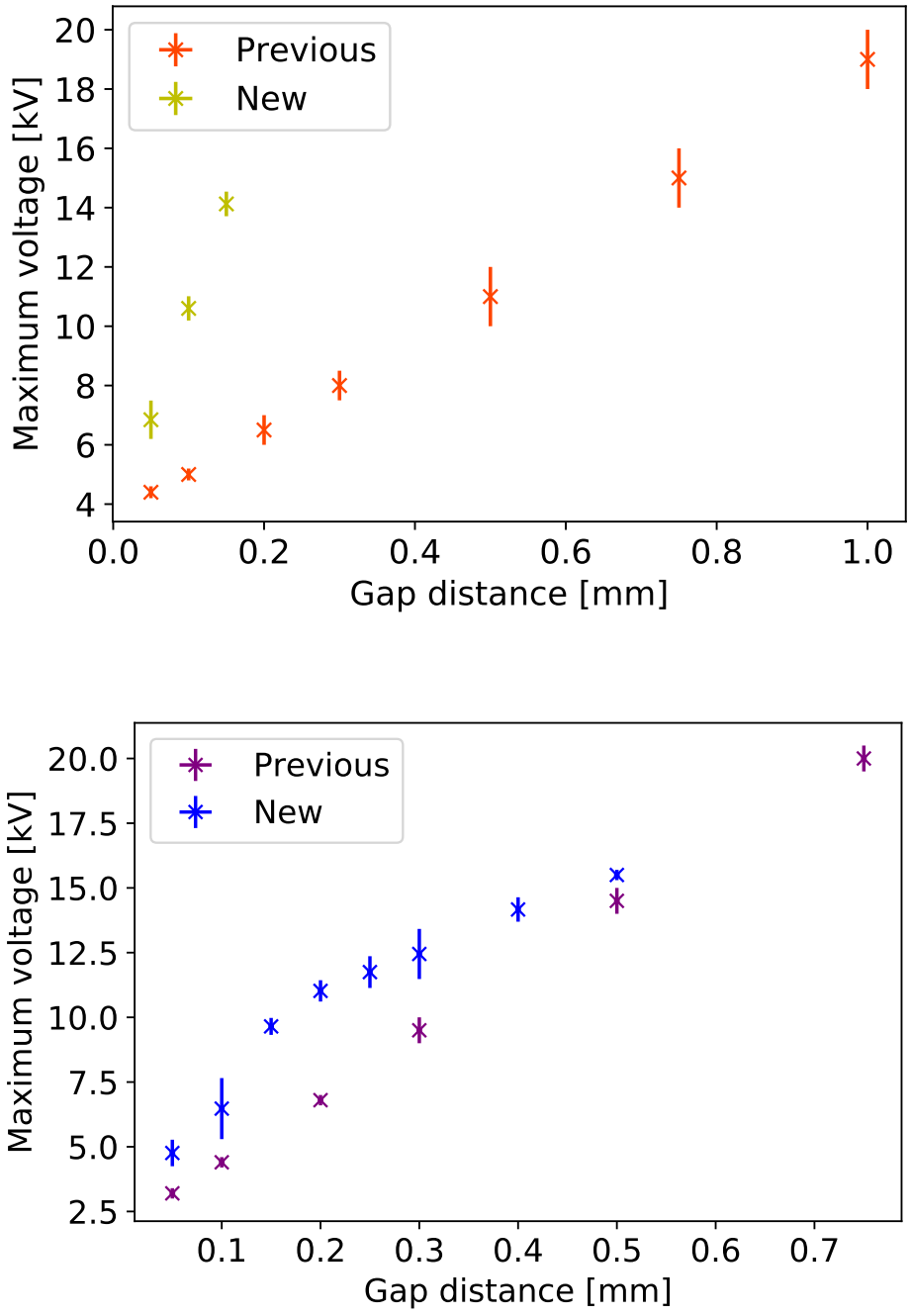


Figure 28: Maximum voltage achieved for the stainless steel electrodes (left) and the coated aluminium electrodes (right). Results from previous and new measurements are shown.

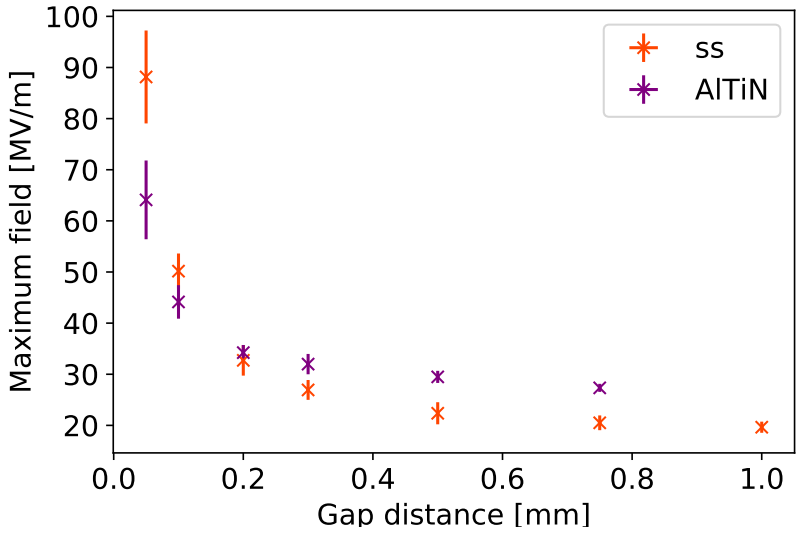


Figure 29: The maximum achievable fields for stainless steel and coated aluminium electrodes from the previous measurements.

are both slightly above 30 MV/m and roughly the same. In the new results the stainless steel can reach a field about 50% stronger than the coated aluminium electrodes according to Figure 18. Additionally it can be seen, that for distances larger than 0.20 mm, the coated aluminium electrodes reach higher fields than the uncoated stainless steel electrodes.
These results again indicate that for small distances the maximum roughness play an important role to determine the maximum field strength. It also shows, that for larger distances the average roughness is more important and therefore coated electrodes will be better than uncoated electrodes.

## 4.5 Extrapolation for larger distances between the electrodes

For the later use in the large experimental setup (c.f. section A) or the prototype ring, much larger distances between the electrodes are needed than measured with this experimental setup. As the obtained results during this thesis are the first results for all four available types of electrodes, these results are extrapolated to distances between the electrodes which are similar to what will be used in the prototype ring.
This extrapolation ignores additional effects that only play a role at larger distances. The first of these effects is that coated electrodes are superior to uncoated electrodes which could already be seen in the previous results. Additionally larger distances mean higher potential differences between the two electrodes. This means that electrons, which are accelerated in the electric field will have higher energies and therefore they might be able to produce an electron avalanche which can cause a breakdown of the electric field. This breakdown can damage the surface. Additionally the particles have higher energies when they hit the electrodes surface which will also cause more damage than for the energies in the latest measurements.
For the prototype ring, flat surface electrodes will be used. Therefore, the FEF is neglected in the extrapolation and the field strength is only calculated by dividing the fitted voltage by the distance[9]. The results obtained are shown in Figure 30.

[9]The large deflectors in the prototype ring also have a FEF, since the assumption of $f = 1$ is only valid for an infinite plate capacitor. Nevertheless it is $f \approx 1$ and therefore the error caused by neglecting the FEF will be smaller than the error which is caused by the additional effects because of the higher electron energies.

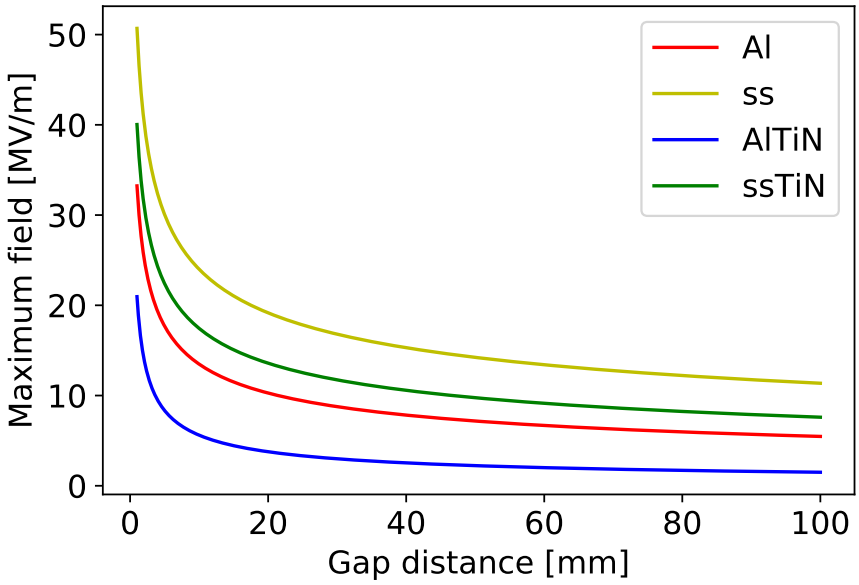


Figure 30: The maximum achievable fields extrapolated to a distance of 100 mm.

According to this extrapolation, the maximum strength which is achievable for the electric field at distances used in the prototype is in the order of several MV/m, which is in the order of what is needed for the prototype ring. As the extrapolated distances are two orders of magnitude larger, this extrapolation can only give a first idea about the maximum field strengths. It is very likely that other effects between the electrodes will also play a role, which are all neglected in this extrapolation based on data from small distances.

# 5 Conclusion and Outlook

During the measurements and analysis for this thesis several things could be learned in terms of handling the electrodes and which electrode type to choose.
Looking at the experimental setup and the way the dark current is recorded it becomes clear that this gives room for improvement as it is done manually up to now.
The behaviour of the current against the applied voltage is as expected. For small voltages the current is zero until the field is too strong. At that point, the current grows exponentially, but no difference between the electrodes can be seen.
The test of reproducibility did not only give the expected results. It could be shown that the setting of the upper electrode does not significantly increase the error on the position or maximum voltage between the electrodes. Two of the three measurement rows also indicate that the results are within an area of below 1 kV reproducible. In the second measurement row an increase of the maximum voltage was measured. It is unclear where this comes from and has to be remeasured, especially as previous measurements did not indicate such a behaviour.
The main focus was put on the maximum voltages that can be applied before a dark current can be measured and therefore the maximum achievable field strengths. As expected, the maximum field strength goes down with distance for all measured electrodes. For both electrode materials the results obtained with the coated electrodes were worse than the uncoated electrodes. This is contradictory to the expectation that the coating with TiN should improve the field quality of the electrodes. Hereby it was noticed that the surfaces of the coated electrodes have a better average roughness than the uncoated ones but also a larger maximum roughness, which is very likely the reason for the worse results. Additionally it could be shown that the stainless steel electrodes reached higher fields than the aluminium electrodes at the measured distances. At this point it would also be interesting to remeasure the surface of the electrodes again now to see how it changed during the measurements.
Comparing the measured results with previous results for uncoated stainless steel and coated aluminium electrodes, measured with the same experimental setup, showed that the maximum fields are much stronger now. This can be explained by an intense cleaning of the vacuum chamber. This indicates that a clean environment is very important for the electrodes to be able to produce a strong field. In the old results also it could also be seen, that at some point the coated electrodes are able to reach higher fields than the uncoated ones, which is in agreement to the expectation based on results from other groups.
An extrapolation of the results was made to get a first impression to see which field strengths might be achievable for distances that are needed between electric bending elements in a particle accelerator. It was stated that the real fields will behave different as other effects will play a role on a larger scale compared to the small scale electrodes, but the extrapolation gives results in the order of what is needed in field strength.
All together it can be said that the results of this thesis show that good surface treatment to get a smooth surface is very important to achieve strong fields with the electrodes. Additionally the vacuum chamber must be very clean, as small amounts of dust already lower the maximum field significantly. As no measurements could be done for distance above 0.5 mm, no answer can be given, which electrode material will be the best for the use of electrostatic bending elements, although the results indicate that stainless steel electrodes are better than aluminium electrodes. To decide which electrodes shall be used, further measurements have to be done at a larger scale setup to get data for realistic distances between the electrodes.
As proposed in chapter 1 a larger experimental setup is planned and already in the status of assembling. This setup shall be used to get more knowledge about strong electric fields at distances which are realistic to be used in an accelerator. Additionally the electric field in this setup is overlaid by a magnetic field to reach conditions which are similar to the prototype ring. More information about this setup can be found in the appendix.

# Bibliography

[1] Bernreuther W. CP violation and baryogenesis. *Lecture Notes in Physics*, 591 pages 237-293, 2002.

[2] Cyburt R. H., Fields B. D., Olive K. A. Primordial Nucleosynthesis in Light of WMAP. *Physics Letter*, B567, pages 227-234, 2003.

[3] Sakharov A. D. Violation of CP Invariance, C Asymmetry, and Baryon Asymmetry of the Universe. *Soviet Journal of Experimental and Theoretical Physics Letters*, 34(5), 1967.

[4] Graner B., Chen Y., Lindahl E. G. and Heckel B. R. Reduced limit on the permanent electric dipole moment of $^{199}$Hg. *Physical Revue Letters*, 116, 2016.

[5] Baron J., Campbell W. C., DeMille D., Doyle J. M., Gabrielse G., Gurevich Y. V. et al. Order of magnitude smaller limit on the electric dipole moment of the electron. *Science*, Vol 343, Issue 6168, 2014.

[6] Pendlebury J. M., Afach S., Ayres N. J., Baker C. A., Ban G., Bison G. et al. Revised experimental upper limit on the electric dipole moment of the neutron. *Physical Revue D*, 92, 2015.

[7] Rosenberry M. A. and Chupp T. E. Atomic electric dipole moment measurement using spin exchange pumped masers of $^{129}$Xe and $^{3}$He. *Physical Revue Letters*, 86, 2001.

[8] Rosenthal, M. *Experimental Benchmarking of Spin Tracking Algorithms for Electric Dipole Moment Searches at the Cooler Synchrotron COSY*. PhD thesis, RWTH Aachen university, 2016.

[9] Fujuyama T. and Silenko A. J. Derivation of generalized Thomas-Bargmann-Michel-Telegdi equation for a particle with electric dipole moment. *International Journal of Modern Physics A*, Vol. 28, 2013.

[10] Ströher H. for the Charged Particle Electric Dipole Moment Collaboration, Feasibility Study for an EDM Storage Ring, proposal, 2019. Can be found under arXiv:1812.08535.

[11] Slim, J. *A Novel Waveguide RF Wien Filter for Electric Dipole Moment Measurements of Deuterons and Protons at the COoler SYnchrotron (COSY)/ Jülich*. PhD thesis, RWTH Aachen University, 2019.

[12] Lenisa, P. at al. Low-energy spin-physics experiments with polarized beams and targets at the COSY storage ring. *EPJ Techniques and Instrumentation*, 6, 2019.

[13] Maier R., Pfister U. and Theenhaus R. for the COSY-Team, The COSY-Jülich Project - May 1990 status. In *Proceedings*. 2nd European Particle Accelerator Conference, Nice, France, 1990.

[14] Lehrach, A., Martin, S., Talman, R. Design of a Prototype EDM Storage Ring. In *Proceedings*. 23rd International pin Symposium, Ferrara, Italy, 2018.

[15] Wille, K. *Physik der Teilchenbeschleuniger und Synchrotronstrahlungsquellen - Eine Einführung*. Springer, 2nd edition, 1996.

[16] Demtröder, W. *Experimentalphysik 2: Elektrizität und Optik*. Springer, 6th edition, 2013.

[17] Russel A. The Electrostatic Problem of two conducting Spheres. *Journal of the Institution of Electrical Engineers*, 65, 1927.

[18] Latham, R. *High Voltage Vacuum Insulation - Basic Concepts ans Technological Practice*. Academic Press, 1st edition, 1995.

[19] Küchler, A. *Hochspannungstechnik - Grundlagen - Technologie - Anwendungen*. Springer, 4th edition, 2017.

[20] Mamun, M. A., Elmustafa, A. A. TiN Coated Aluminium Electrodes for DC High Voltage Electron Guns. *Journal of Vacuum Science & Technology A*, Vol 33, 2015.

[21] See https://www.cybertechnologies.com/de/ for measurement device CT 300 [Last called 25.10.2019].

[22] Böll, J. (FZ Jülich), Private communication, January 2019.

[23] Grigoryev K., Rathmann F., Stahl A., Ströher H. Electrostatic deflector studies using small-scale prototype electrodes. *Review of Scientific Instruments*, 90, 2019.

[24] See https://www.uhvdesign.com/ for linear drive CLSM38-50-H-DLA [Last called 02.10.2019].

[25] See https://www.heinzinger.com/products/high-voltage/universal-high-voltage-power-supplies/ for Heinzinger PNC 30000 [Last called 02.10.2019].

[26] See https://www.tek.com/ for Picoamperemeter Keithley 6485 [Last called 02.10.2019].

[27] See https://tdk-electronics.tdk.com for EPCOS EC90X and EC600X [Last called 02.10.2019].

[28] See https://tdk-electronics.tdk.com for diodes of type BAV199 [Last called 02.10.2019].

[29] See https://www.agilent.com/ for TriScroll 300 [Last called 02.10.2019].

[30] See https://www.agilent.com/ for TwisTorr 304 [Last called 02.10.2019].

[31] See https://www.agilent.com/ for Vaclon Plus 300 [Last called 02.10.2019].

[32] See https://www.vacom.de for UHV valve Vacom 5GVM-160CF-MV-S [Last called 02.10.2019].

[33] Grigoryev, K. Deflector Development, 14th JEDI collaboration meeting March 11th and 12th 2019, Jülich, Germany.

[34] Demary, N. (FZ Jülich), Private communication, April 2019.

[35] Rogowski, W. Die elektrische Festigkeit am Rande des Plattenkondensators. Ein Beitrag zur Theorie der Funkenstrecken und Durchführungen. *Archiv für Elektrotechnik*, 12, 1923.

[36] Grigoryev, K. (FZ Jülich), Private communication, September 2019.

# A Large electromagnetic test bench

As proposed before, a new experimental test bench is planned and in the status of assembling at the moment. This setup will feature distances which are similar to what will be used in the prototype ring for the EDM measurement. It will also include a magnetic field, as planned for the prototype ring, to see how the fields influence each other. This magnetic field is needed in the prototype ring, to "freeze" the spin as described in 2.2. The overlaying fields can be achieved by inserting the electrostatic deflectors inside a electromagnet as shown in Figure 31.

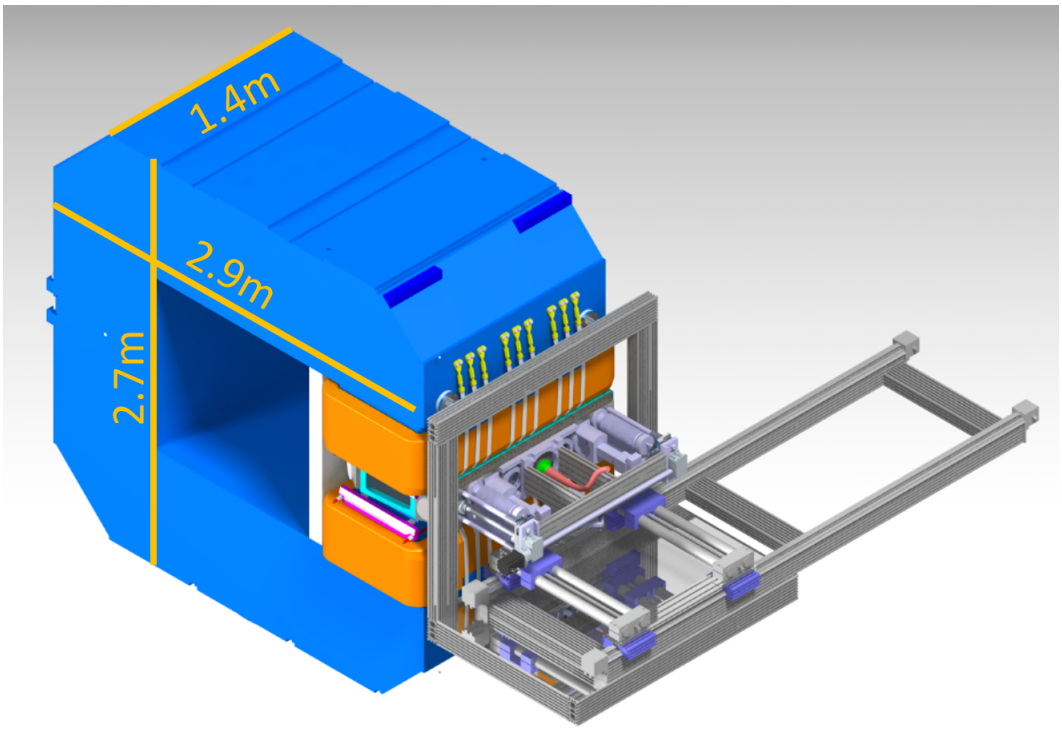


Figure 31: CAD drawing of the large setup inside the magnet with the support structure at the front [34].

The rails in front of the magnet are used for mechanical support during installation. The part that is inserted inside the magnet contains the electrodes. A schematic view of this is shown in Figure 32.

The electrodes (component 1 in Figure 32) are produced out of aluminium and coated with titanium nitride. They have a length of 1020 mm, a height of 90 mm and a thickness of 30 mm. For cost reasons only one pair is produced, which is shown in Figures 33 and 34.

To create the best homogeneity for the electric field, the electrodes have to follow a Rogowski profile [35]. For machining reasons, this profile is approximated by round edges. The inner edges of the electrodes are rounded with a radius of 18 mm and the outer edges have a radius of 10 mm.

Both electrodes in the setup are mounted on a HV feed trough (component 2 in Figure 32) and two actuators (component 3 in Figure 32) which are used to set the distance between the electrodes.

As already mentioned, the whole setup is installed inside a magnet to have an overlay of electric and magnetic field. The larger distances between the electrodes mean that also the potential difference between the electrodes will increase. This will have the effect that particles such as dust or electrons, which are accelerated from one electrode towards the other have a higher kinetic energy. Simulations have shown, that the magnetic field will change

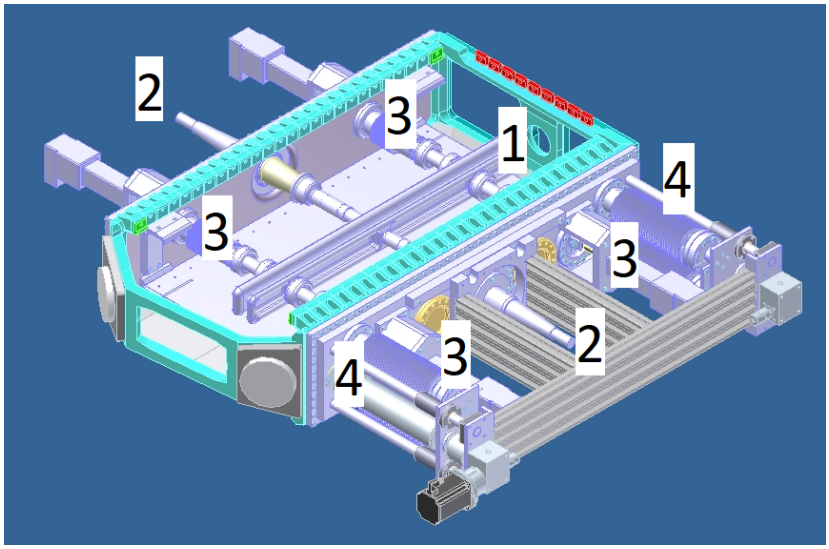


Figure 32: CAD drawing of the proposed setup with larger electrodes [34]. 1: the two deflectors, 2: high voltage feed through, 3: actuator to change the gap distance, 4: foil stiffeners.

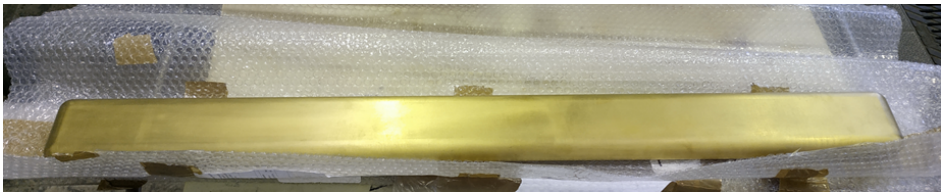

Figure 33: Picture of one of the new electrodes before mounting on the flange [36].

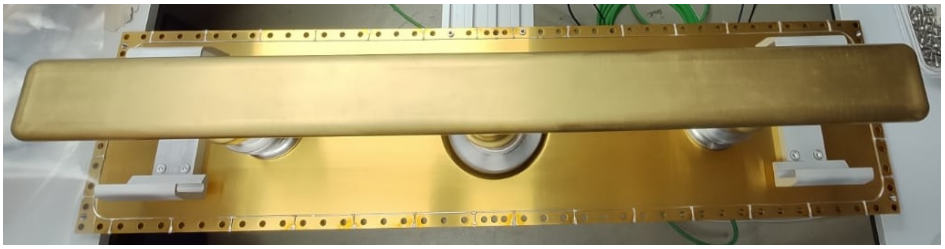

Figure 34: Picture of one of the new electrodes mounted on the flange. Taken from [36], cut.

the path of the accelerated particles [23]. Instead of hitting the other electrode, they will be deflected towards the top or the bottom of the chamber, following the magnetic field line. To protect the vacuum chamber which is surrounding the electrodes[10] a titanium foil (not displayed for the top layer) is mounted on top and bottom of the vacuum chamber. Four foil stiffeners (component 4 in Figure 32), two for each foil, are mounted at the front of the setup to keep the foil stiff.
The electrodes in this setup can be spaced with a gap of 20 mm to 120 mm which is similar to what will be used in the prototype ring. For each electrode an individual power supply is available with a range of $V = \pm 200\,\mathrm{kV}$ each. The aim of this setup is to reach stable fields without any dark current in the order of $E = 8\,\mathrm{MV/m}$.
The current status of this setup is that most parts are already installed on the flanges or even in the vacuum chamber. It is planned to finish the assembling at the end of this year and perform first measurements next year.

[10] A single spark to the chamber would probably not cause any significant damage to it. Since the chamber inside the magnet can not be changed easily, it is favourable to protect it by an easy exchangeable part.

## Acknowledgements

On the last page of my thesis I would like to thank everyone who helped me during the work on my thesis.
First of all I want to give a very big thank you to Prof. Dr. Andreas Lehrach who gave me the possibility to write this thesis under his supervision. Another big thank you goes to Prof. Dr. Lutz Feld who was willing to be the second superviser.
Many thanks also go out to Dr. Kirill Grigoryev, with whom I worked together on the electrostatic deflectors. He helped me with all my problems and explained me all the things I needed. Another thank you goes to Nils Demary and the workshops in FZJ, who were willing and able to fix all problems that occurred while assembling the new setup with large electrodes.
Special thanks also go to the other students in IKP with whom I had many discussion and nice moments. Here specially want to mention my fellow master students Abhiroop Sen, Achim Andres, Beñat Alberdi, Mathis Beyß and Saad Siddique. Also a big thank you to PhD student Vera Ponzca who helped me with a lot of problems that occurred during the year.
My final thank you goes to my family and Anna von Byern, who always supported me during the last year and cheered me up after a bad day in the laboratory. Thank you.

# Selbstständigkeitserklärung

Ich versichere hiermit, dass ich die Arbeit selbstständig verfasst und keine anderen als die angegebenen Quellen und Hilfsmittel benutzt sowie Zitate kenntlich gemacht habe.

Ort, Datum | Unterschrift

# Statement of authorship

I hereby certify that I have done this work independently and without the use of any aids other than those specified. All parts which are taken literally or analogously from published and not published writings of others, are marked as such.

Place, Date | Signature